Disturbance Estimator Based Predictive Current Control of Grid-Connected Inverters

Ahmed Samawi Ghthwan Al-Khafaji

Submitted to the
Institute of Graduate Studies and Research
in partial fulfillment of the requirements for the Degree of

Master of Science
in
Electrical and Electronic Engineering

Eastern Mediterranean University
June 2013
Gazimağusa, North Cyprus

Approval of the Institute of Graduate Studies and Research

Prof. Dr. Elvan Yılmaz
Director

I certify that this thesis satisfies the requirements as a thesis for the degree of Master of Science in Electrical and Electronic Engineering.

Prof. Dr. Aykut Hocanın
Chair, Department of Electrical and Electronic Engineering

We certify that we have read this thesis and that in our opinion it is fully adequate in scope and quality as a thesis for the degree of Master of Science in Electrical and Electronic Engineering.

Prof. Dr. Osman Kükrer
Supervisor

Examining Committee

1. Prof. Dr. Hasan Kömürcügil
2. Prof. Dr. Osman Kükrer
3. Prof. Dr. Şener Uysal

ABSTRACT

The work presented in my thesis considers one of the modern discrete-time control approaches based on digital signal processing methods, that have been developed to improve the performance control of grid-connected three-phase inverters.

Disturbance estimator based predictive current control of grid-connected inverters is proposed. For inverter modeling with respect to the design of current controllers, we choose the d-q synchronous reference frame to make it easier to understand and analyze. In accordance with the d-q system coordinate, we select the space vector pulse-width modulation (SVPWM) to implement the drive logic of the electronic switches, which is considered the best method used to generate the PWM control pulses because it provides a fixed switching frequency. Therefore, the distortion in the output voltage and current is to be less compared with the other PWM methods.

In this thesis, we discuss the basics of grid-connected inverter modeling and analysis. In addition, all the equations have been derived in (abc) and (dq) reference frames. The simulations of predictive current control and disturbance estimator are discussed. In the simulation study, we obtain grid current waveforms in the steady-state and for step changes in the d-component of the reference current. The controlled grid current is observed to track the desired current with negligible differences. The grid angle is extracted via PLL using the estimated reactive disturbance component. Moreover, the

stability of the disturbance estimator due to the parameter errors in the inductor filter is analyzed numerically regarding the estimator gains.

The advantage of this strategy comes from the fact that grid voltage sensors are not required, thus we obtain a low-cost implementation with high performance and robustness.

Keywords: Inverters, Predictive Current Control (PCC), d-q Synchronous Reference Frame, Space Vector (PWM)

ÖZ

Bu çalışmanın amacı, şebekeye bağlı 3-faz inverterlerin başarımını iyileştirmek için son zamanlarda geliştirilen, sayısal işaret işleme tabanlı, kesikli-zaman kontrol yaklaşımlarını incelemektir.

Şebekeye bağlı inverterlerin bozanetken kestirimli öngörülü akım kontrolü için bir yöntem önerilmektedir. Akım kontrolünün daha anlaşılır ve analizinin daha kolay olması açısından d-q senkron referans çerçevesi seçilmiştir. Bu çerçeveye uygun olarak, elektronik anahtarların darbe genişliği kiplemeli (DGK) kontrol sinyallerini üretmek için uzay vektörü DGK'si seçilmiştir. Bunun bir nedeni de bu yöntemin sabit anahtarlama frekansına sahip olmasıdır. Bunun sonucunda çıkış gerilimi ve akımındaki bozunumun diğer DGK yöntemlerine göre daha az olması beklenir.

Bu tezde şebekeye bağlı inverterlerin modelleme ve analizinin temelleri tartışılmıştır. Bütün denklemler (abc) ve (dq) çerçevelerinde çıkarılmıştır. Öngörülü akım kontrolü ve bozanetken kestirimcisinin benzetimleri de tartışılmıştır. Benzetim çalışmalarında, şebeke akımının durağan durum ve referansın d-bileşenindeki akım değişimi durumlarında dalga şekilleri elde edilmiştir. Kontrol edilen akımın istenen akımı çok az farkla takip ettiği gözlenmiştir. Daha sonra, PLL uygulamak suretiyle bozanetken kestiriminin reaktif bileşenini kullanarak şebeke faz açısının elde edilmesi tartışılmıştır. Son olarak ise, bobin süzgeç ve kestirimci kazançlarındaki parametre hataları durumunda bozanetken kestiriminin kararlılığı, sayısal olarak incelenmiştir.

Bu yaklaşımın bir üstünlüğü de, şebeke gerilim duyargalarına ihtiyaç duymamasıdır. Dolayısiyle yüksek başarımı olan ve çalışması istikrarlı bir sistem düşük maliyetle elde edilmektedir.

Anahtar kelimeler: Inverterler, Öngörülü Akım Kontrolü, d-q Senkron Referans Cerçeve, Uzay Vektörü DGK

To My Beloved Mother

ACKNOWLEDGMENTS

I would like to express my sincere appreciation and thanks to my supervisor Prof. Dr. Osman Kükrer for his continuous support and guidance during the execution of my thesis.

I would like to thank the chairman of Electrical and Electronic department Prof. Dr. Aykut Hocanin for his many supports and fatherly advices.

My special thanks go to my love, Shamim, who was always stood by me during my studies.

I would like to express my greatest appreciation towards my mother and my siblings, for their invaluable love and support.

TABLE OF CONTENTS

LIST OF TABLES

LIST OF FIGURES

LIST OF SYMBOLS AND ABBREVIATIONS

α	Space Vector Angle
δ	Pulse Width Duration
θ	Grid Angle
φ	Current Phase Shift Angle
λ	Eigenvalue
ADC	Analog to Digital Converter
BJT	Bipolar Junction Transistor
CC-VSI	Current Control Voltage Source Inverter
CSI	Current source Inverter
DSP	Digital Signal Processing
DT	Dead Time
FCS-MPC	Finite Control Set Model Predictive Control
GM	Gain Margin
GTO	Gate Turn-off Thyristor
HB	Hysteresis Band
IGBT	Insulated-Gate Bipolar Transistor
LTI	Linear Time Inversion

MOSFET	Metal Oxide Semiconductor Field Effect Transistor
PC	Predictive Control
PCC	Predictive Current Control
PI	Proportional-Integral
PLL	Phase Locked Loop
PM	Phase Margin
PV	Photovoltaic
PWM	Pulse Width Modulation
QSW	Quasi Square Wave
RPCC	Robust Predictive Current Control
SVM	Space Vector Modulation
SVPWM	Space Vector Pulse Width Modulation
SW	Square Wave
TF	Transfer Function
THD	Total Harmonics Distortion
VSI	Voltage Source Inverter

Chapter 1

INTRODUCTION

1.1 Renewable Energy

Renewable energy is that type of energy which comes from natural sources of energy which are continuously available such as; solar, wind, tide and waves. All these sources can be used to support the grid by electricity. The final statistic report indicate to about 20% of the global energy which is used for lighting, heating, and power application comes from the renewable energy resources.

The main reasons why the research interest is noticeably increased in the field of renewable energy are; firstly, the wide geographic locations which help to investigate in this field of renewable (could be available in many places) when compared with the other sources of energy, for instance oil and gas. Secondly, with the appearance of modern technologies in the field of manufacturing and alternative energy production with the ease of installation and maintenance, all of these advantages led to increase investment in this area.

We notice the various advantages of renewable energy. The problem now is how to obtain the energy from these resources, and what we are going to discuss in this thesis is one way among many several ways; of how to satisfy a high power quality with high

efficiency and high performance requirements. Here we are going to use current control strategy and grid synchronization to achieve our goal.

1.2 Inverters

An inverter is a device which is used to convert static power (constant voltage, constant current) to another form called dynamic power (AC Power); which means that the voltage and current have variable values with respect to time.

Inverters can be classified into many types, depending on the application purpose. Generally, there are two main types of inverters: single phase and three phase inverters. These two types belong to two families; voltage source inverter (VSI) and current source inverter (CSI). Usually VSI are connected with fixed source voltage battery or photovoltaic source, therefore it's used at the application where low and medium power is needed. On the other hand, CSI is used for high power loads and medium voltage.

Generally, single phase inverters are used to supply loads which need small or medium current, for example, single phase induction motor. Three phase inverters are usually used with high power applications, which may require high currents and voltages. There are many important characteristics to measure the inverter quality, which can be listed as given in [1]:

- High performance and efficiency.
- High power factor.
- High torque when used to drive 3phase induction motors.
- No need for filter when used to feed nonlinear load (rectifier).

- Low total harmonic distortion (THD).

1.2.1 Single Phase Bridge Inverter

Figure 1.1 shows the general construction of a single phase bridge inverter. The inverter consists of four electronic switches; here we used IGBT transistor each one connected with antiparallel diode. These diodes are more important when the load is inductive; it passes the negative load current and used as a protection device at switching period. Also, it's possible to use any other electronic switch (e.g. BJT transistor, GTO thyristor and MOF transistor, each power transistor operates at maximum time period equal to (*T/2*), since $T = 1/f_s$, such that f_s is switching frequency.

The control circuit for the inverter should be designed to achieve the following states:

- (Q1 ,Q3) ON state when (G1, G3) is logic 1, and OFF state when (G1, G3) is logic 0.
- (Q2, Q4) ON state when (G2, G4) is logic 1, and OFF state when (G2, G4) is logic 0.
- (Q2, Q4) turn OFF before some micro second than (Q1, Q3) turns ON.
- (Q2, Q4) turns ON after (Q1, Q3) turns OFF in order to prevent any damage that could happen to the transistors in the same leg [2].

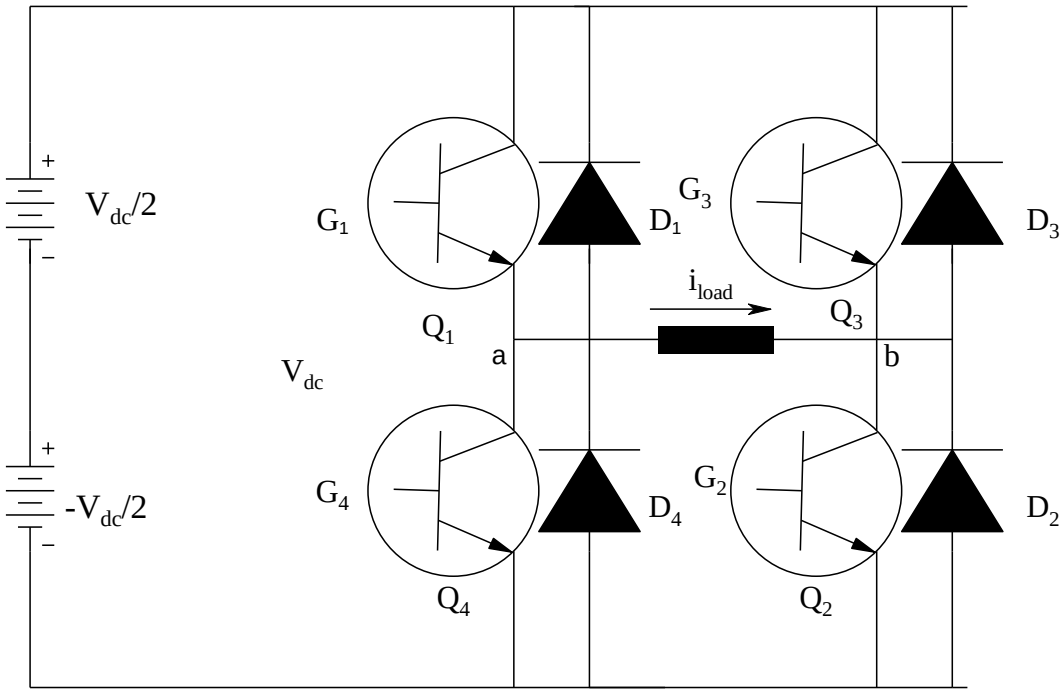

Figure 1.1: Single Phase Bridge Inverter [2]

Figure 1.2(b) shows the general construction of a three-phase half bridge inverter. This is a combination of three single-phase half bridge inverters shown in Figure 1.2(a). All three legs operate together to satisfy the voltages synchronization, i.e. $120°$ phase shift between each phase. The control circuit designed to drive these transistors has the same properties with the output voltage waveform, for instance if (Q1) conducts at $\theta = 0$ the pole voltage V_{aN} changes from zero to $V_{dc}/3$ when the load is WYE connected, and transistor conducts until half period π; the transistor becomes off again until the second period starts at $\theta = 2\pi$. This is called normal operation, but the same application is required such that each transistor conducts for a period equal to $2\pi/3$ (or may be less). All these methods give square signals in the output, moreover the output waves may be two level or multilevel. In order to be clearer we can demonstrate the more popular two types considered as basic in three phase inverters.

- **(180°) Conduction System.**

In this case each transistor conducts (180°), the phase and line voltage waveforms depend on the kind of connected load; if it is delta or WYE. Also the phase shift between voltages and currents depend on the load (R or RL), as shown in figure 1.2(c).

- **(120°) Conduction System.**

In this case each transistor conducts (120°), the output line voltages are quasi square waves (QSW) [3].

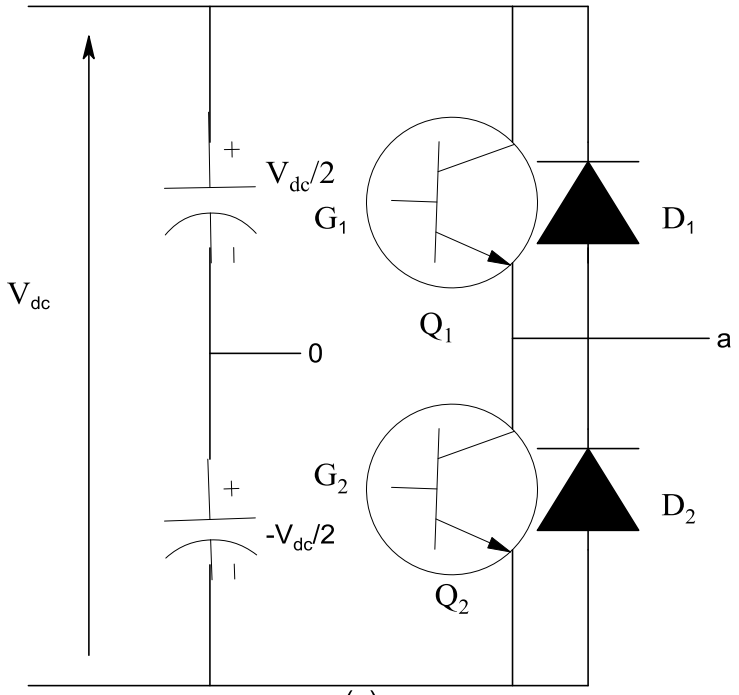
+
$V_{dc}/2$
G_1
D_1
V_{dc}
Q_1
0
a
G_2
+
D_2
$-V_{dc}/2$
Q_2

(a)

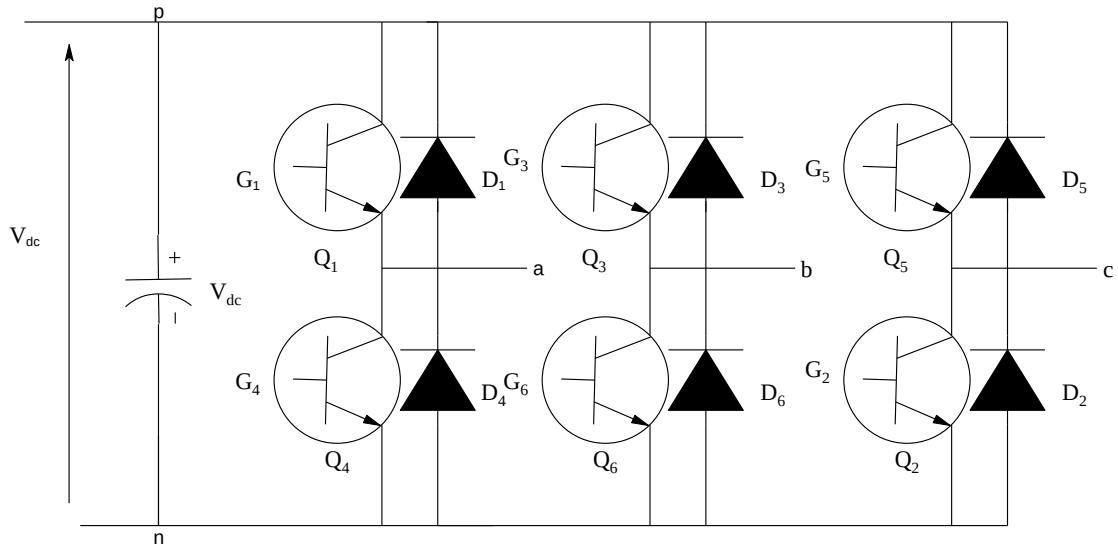
p
V_{dc}
G_1
D_1
G_3
D_3
G_5
D_5
Q_1
a
Q_3
b
Q_5
c
+
V_{dc}
G_4
D_4
G_6
D_6
G_2
D_2
Q_4
Q_6
Q_2
n

(b)

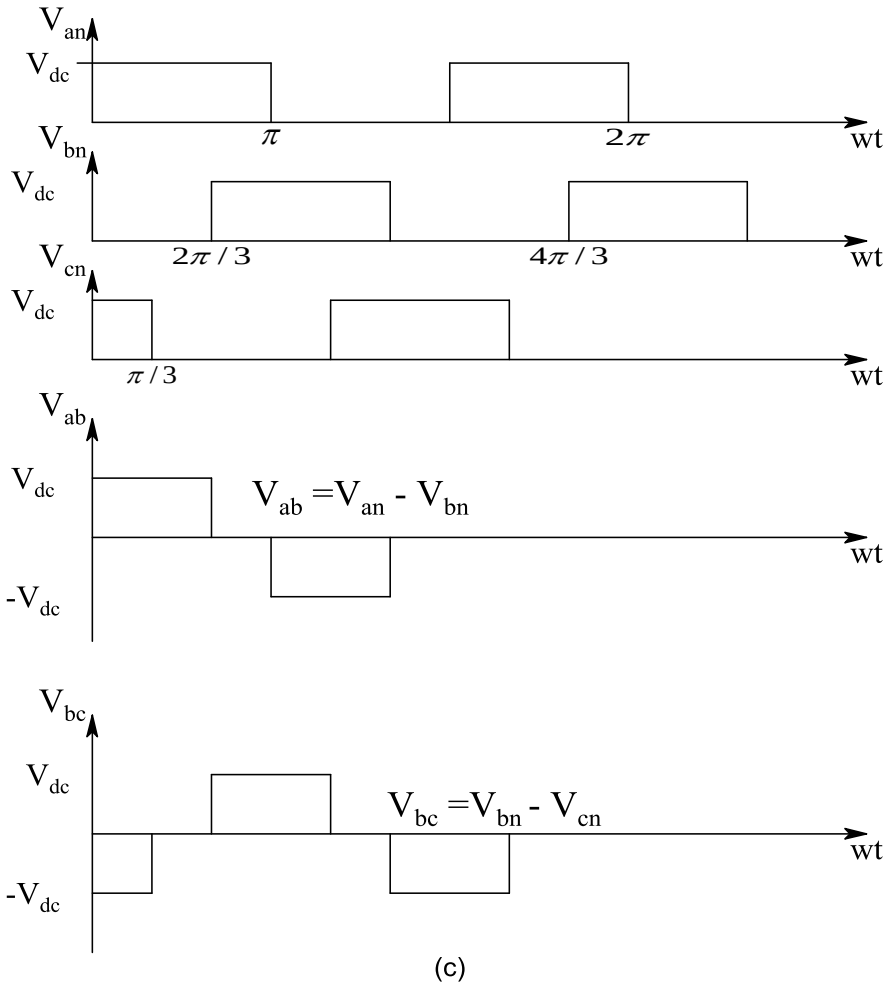

Figure 1.2: (a) Single-Phase Half Bridge Inverter, (b) Three-Phase Half Bridge Inverter, and (c) Output Voltages Waveforms [1]

1.3 Pulse Width Modulation (PWM)

Pulse width modulation is one of the techniques commonly used to drive the power electronics switches such as transistors. The principle of this method is explained as follows; the DC voltage source is "chopped" by the power electronics devices which are connected to the inverter. The pulses generated from this technique have the same amplitude and different pulse width duration (δ) which depend on the comparator circuit design. The main advantage of the PWM technique compared with the square

wave is the reduction of the total harmonic distortion, which comes from the effective harmonics [4].

There are several types of the PWM method and each one has advantages and disadvantages. Here we will describe the basic and most common techniques.

1.3.1 Sinusoidal PWM (SPWM)

In this technique the input signals to the comparator circuit are triangular signal (carrier) in the reference signal, and sinusoidal ($V_{control}$) in the other one. When the reference becomes larger than the sinusoidal signal, the inverter output voltage is $-V_{dc}/2$, and when the $V_{control}$ is larger than carrier signal the inverter output voltage is $+V_{dc}/2$ as shown in Figure 1.3 shown the inverter output voltage of the single phase half bridge inverter shown in Figure 1.2.a, in three phase inverters the control circuit designed to compare between the carrier and three phase sinusoidal signals, than we used only one control circuit to generate the control pulses [5].

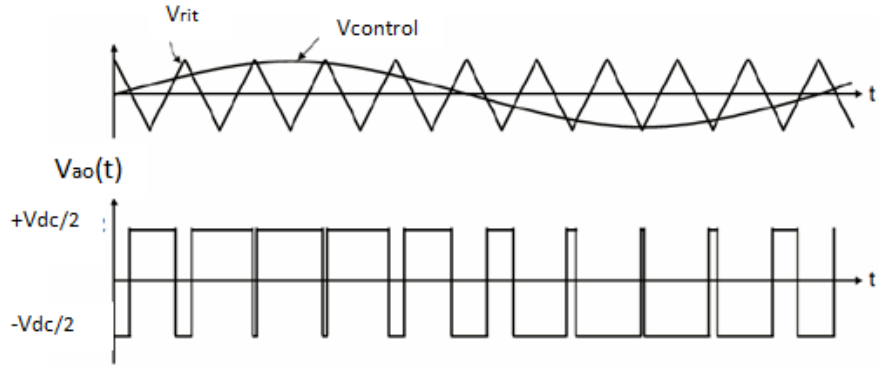

Figure 1.3: PWM [5]

1.3.2 Hysteresis Band Current Control PWM

In this type of the PWM techniques the three-phase inverter needs three sets of the control circuit similar to the one shown in Figure 1.4(a) to generate the control pulses. The aim of this method for basic operation is that the actual current continually tracks the control current inside a hysteresis band HB. In this case the width of the HB is very important to adjust the switching frequency and peak-to-peak current ripple. When the HB is small the switching frequency increases and the current ripple decreases. Then, for the system to work in the best operation the optimal band should be selected that maintains a balance between the harmonic ripple and inverter switching loss is desirable [2].

Figure 1.4.b shows the principle of HB current control operation; the control circuit generates the sine reference current wave of desired magnitude and frequency, and it is compared with the actual phase current wave. As the current exceeds a prescribed HB, the lower transistor in the half –bridge Figure 1.2.a is turned ON and the upper transistor is turned OFF the inverter output voltage change from $+V_{dc}/2$ to $-V_{dc}/2$.

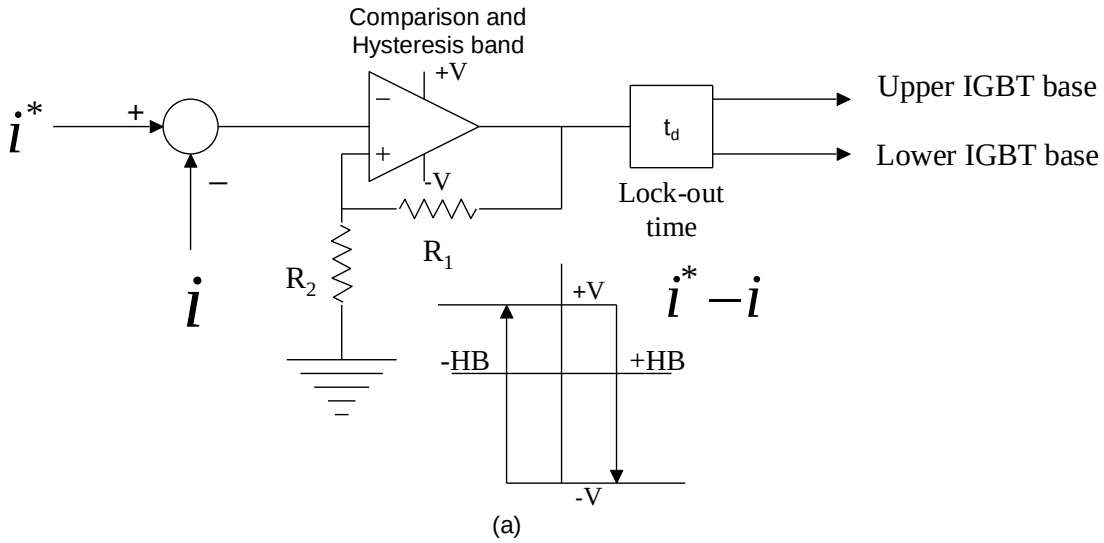

(a)

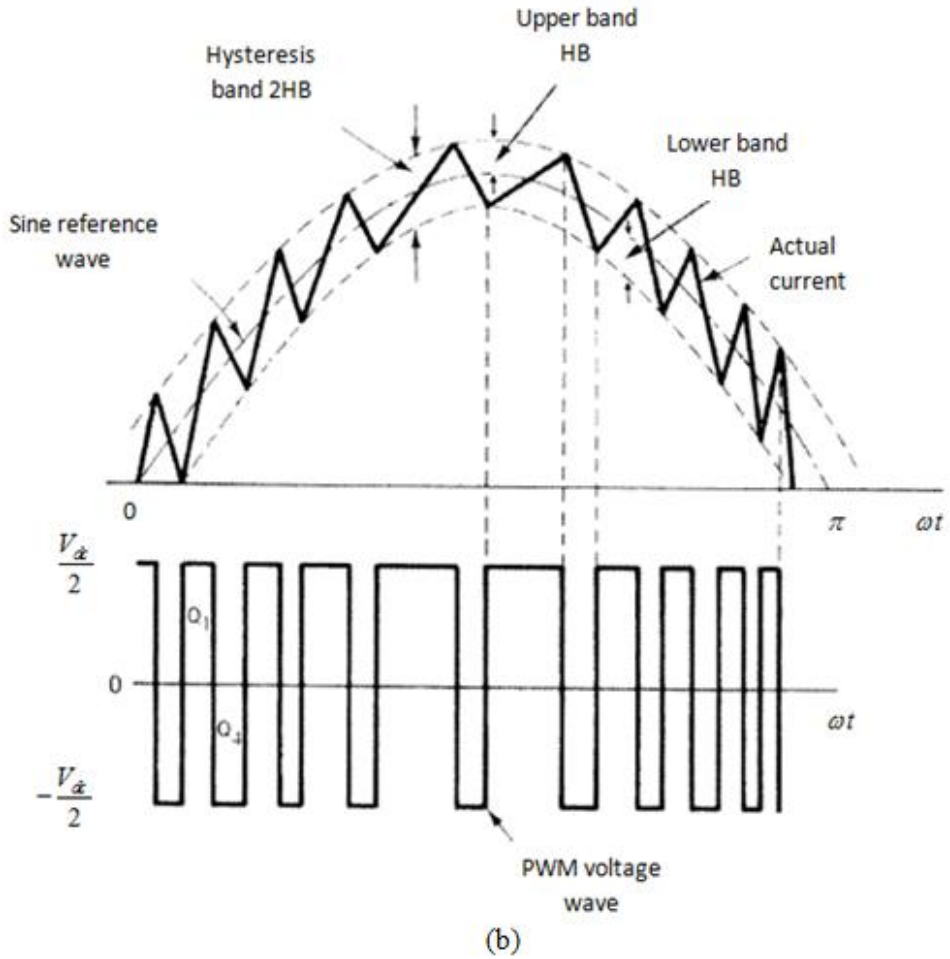

(b)

Figure 1.4: (a) Control Block Diagram for the HB-PWM and (b) Principle of HB-CC [2]

1.3.3 Space-Vector PWM (SVPWM)

This type of techniques I will explain in Chapter 3 with all detail.

1.4 Thesis Organization

This thesis is organized as follow; in Chapter 1, we introduce the basic environmental sources needed in renewable energy used for grid enhancement to reduce global warming and summarize inverter control techniques. In Chapter 2, an overview of some of the current control strategies known as predictive current controllers will follow. In Chapter 3, we describe the typical modeling of three phase inverters, and illustrate the continuous equations. Chapter 4 is considered with Chapter 5 are considered the core of this thesis. In Chapter 4 we explain the discrete equations for predictive current and closed-loop voltage control. In addition, we discuss the system stability. Simulation results are given in Chapter 5. Conclusion and future work are given in Chapter 6.

Chapter 2

REVIEW OF PREDICTIVE CURRENT CONTROL METHODS

In this chapter we are going to discuss some of the new methods used in controlling power converters, called predictive current controllers. All these methods are invented to overcome the problem arising from the variation of system parameters affecting the shape of the load current and system stability. In addition, most of the control systems are implemented by using digital microcontrollers [6].

2.1 Finite Control Set Model Predictive Control (FCS-MPC)

FCS-MPC is a new technique used in power converters. This type of controller requires in practical application the correct compensation of the computation delay. This compensation demands load current estimation, commonly achieved in the open loop method. But, this method gives high waveform distortion with existing parameter variation. The method proposes to minimize effects of the variation by using a 'Luenberger observer', which is a particular estimation observer involving a sample of the error of the prior estimation in the current repetition.

In [7]-[8], it is proposed to involve a state observer to keep the distortion at minimum, by predicting a new state which can be considered to be a future state in closed-loop

method. In this way this is considered to be the first modification to give the system more robustness.

2.1.1 Predictive Model

It is necessary to choose which model is appropriate for the entire system, by classifying these models into inverter voltage model and load current model. In future states the load current model is used to predict the load current and we need to compute the cost function by computing the finite states via the inverter voltage model.

- **Load current model**

The circuit shown in Figure 2.1 depicts the electrical circuit of the load model description. Inverter output voltage is $V_0(t)$, the grid voltage is $V_g(t)$ and L, R are the interconnector parameters. From Figure 2.1, we can derive the current control differential equation as follows.

$$\frac{d}{dt} i_o(t) = \frac{1}{L}(V_o(t) - V_g(t) - \frac{R}{L} i_o(t)) \tag{2.1}$$

$$\left(\frac{di_o}{dt}\right)_{t_k} = \frac{i(t_{k+1}) - i(t_k)}{T_s} \tag{2.2}$$

Equation 2.2 represents the forward approximation substitute to obtain (2.3), T_s represent the sampling period.

$$i_o[t_{k+1}] = (1 - \frac{RT_s}{L}) i_o[t_k] + \frac{T_s}{L}(V_o[t_k] - V_g[t_k]) \tag{2.3}$$

Where $i_L[k]$ and $V_g[k]$ are the two variables that are considered the most important for predictive control. So, the quality of the prediction is connected directly with the model parameter accuracy.

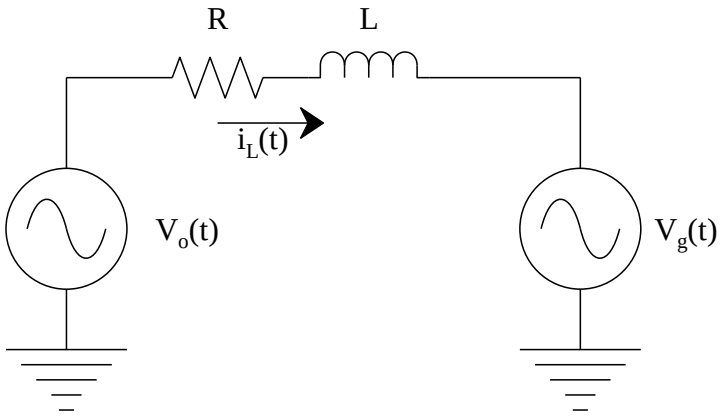

Figure 2.1: Electrical Circuit of the Load Model [6]

- **Inverter voltage model**

Figure 1.2(b) shows a two level VSI consisting of six power transistors, two in each leg, controlled by switching functions (S_a, S_b, S_c). The phase voltage can be expressed as.

$$V_{abc} = (2 \times S_{abc} - 1)\frac{V_{dc}}{2} \tag{2.3}$$

$$S_{abc} = [0,1]$$

Equations (2.2, 2.3) illustrate that the load current trajectory is affected by the power electronic switches position. Moreover, three phase inverter has six possible states, two states for each leg and each two switches common in one node. Practically the mission of the controller is to make dealing with the three currents out from the three nodes by controlling each phase independently of the two other phases [6]. In the final the combined results of the six states and their corresponding future current state predictions, these are considered the inputs of an optimization algorithm, which calculates the next control action to be applied.

- **Optimization**

In this action we want to get minimum cost function thereby, the predictive model should be known in the manner that offers a number of possible paths for which inputs can be applied to the system. So, the optimization form of the cost function can be expressed as

$$J = \left| i_L^* - i_L \right|_{abc} \tag{2.4}$$

i_L^*：Reference current.

2.1.2 Estimation Observer

The estimated current is.

$$\hat{i}_L[k+1] = (1 - \frac{R_L T_S}{L_L})\hat{i}_L[k] + \frac{T_S}{L_L}(V_i[k] - V_g[k]) + K\hat{e} \tag{2.5}$$

$\hat{e} = i_L(k) - \hat{i}_L(k)$ represents the error value between the actual and estimate current, and K is the observer gain.

2.2 Robust Predictive Current Control (RPCC)

In [9] proposed a new method for CC in three-phase grid-connected inverters. The control combines a two-sample deadbeat control law with a Luenberger observer to estimate the future value of the grid currents. The resulting control offers robustness against the computational delay inherent in the digital implementation and considerably enhances the gain and phase margins of the previous predictive controls while maintaining the high-speed response of the deadbeat controllers.

The control circuit of the CC-VSI has two missions [10], [11]: regulate the dc- bus voltage and transfer the generated power to the grid with a unity power factor. The last condition implies a low harmonic distortion (less than 5%) on the inverter output currents and unity displacement factor.

The line currents effect directly when any change happen in the grid voltage [12]. If the control is not fast enough to change the inverter PWM transients with over-current may occur. That is the reason why grid-connected inverters require fast current controllers. [13], [14], [15], offer the fastest response. However, due to their high bandwidth, the stability of the deadbeat controllers is often compromised by the calculation delay inherent in the digital implementation or variations on the filtering inductance.

Figure 2.2 sampling can be performed either before the calculation interval at point A ($t_d > T_s$), and point B ($t_d < T_s$), this case is similar to the ideal control; however, it leaves a small reserve time for computation. Both cases are regarded by defining the delay .

$$t_d = T_d + m.T_s \tag{2.6}$$

$$T_d < T_s, m = [0,1]$$

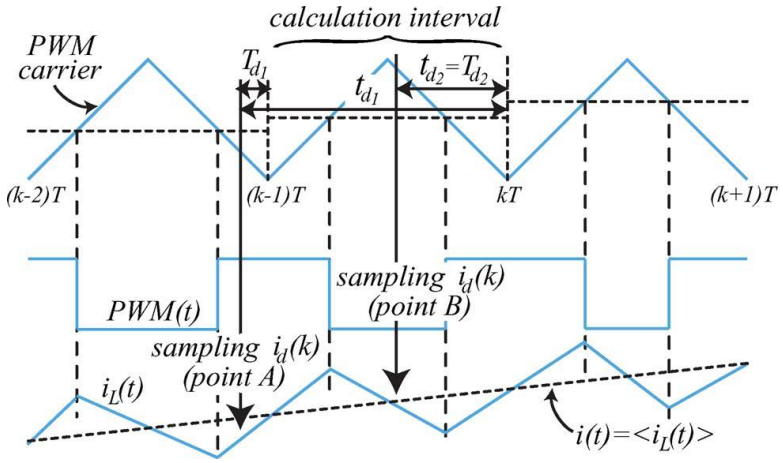

Figure 2.2 : Sampling Options: Before the Calculation Interval (point A) or During the Calculation Interval (point B) [9]

2.2.1 Deadbeat Controllers Analysis

The linear time invariant (LTI) system is to be stable in (n) sample with respect to the system order. For instance with order equal to (n), and applying a suitable deadbeat control law, we can clarify this method in two steps as follows:

2.2.1.1 One-Sample Deadbeat

This type is just used with the fist-order system and the typical controller stabilizes in just one sample and the sampling must be done in the same calculation period and delay T_d compared with T_s. The present between T_d / T_s it know by ε, to find the control low. First, assume $\varepsilon = 0$, the delay inverter current $i_d(t) = i(t - t_d)$, $v_{gd}(t) = v_g(t - t_d)$, where t_d is the delay time.

$$v_o(k) = \overline{v}_{gd}(k) + \frac{L_n}{T_s}.(i_{ref}(k) - i_d(k)) \qquad (2.7)$$

Where L_n is the nominal inductance value, $\overline{v}_{gd}(k)$, is three successive samples of $v_{gd}(k)$ which can be evaluated as;

$$\bar{v}_{gd}(k) = \frac{3}{2} v_{gd}(k) - \frac{1}{2} v_{gd}(k-1) \tag{2.8}$$

The previous step observes the computation of $\bar{v}_{gd}(k)$, that leads us to know which behaves as a forward input to the control to move the grid-voltage disturbance this makes the output current independent of the grid voltage in the close loop system.

$$H(z) = \frac{i_d(k)}{i_{ref}(k)} = \frac{L_n}{L} . \frac{1}{z-1} \tag{2.9}$$

2.2.1.2 Two-Sample Deadbeat ("predictive controllers")

Sampling before the computing interval (point A) in Figure 2.2, the whole next period is available to solve the control calculations, however, the power stage order increases by one. Regularly, the analog signals are converted into digital signals using (ADC_s) are processed in parallel with the computation of the prior interval, adjusting the prompt of the three current results before the prior interval ends at $(k-1)T_s$. This mean $T_d << T_s$ or $\varepsilon = 0$. This method has more advantages when using a fixed PWM, moreover, the current sensed is very close to the average current $i(t)$ shown in Figure 2.2, which eliminates hen, no need to use filters.

$$i_d(t_{k+1}) = i_d(t_k) + \frac{T_s}{L}(v_i(t_{k-1}) - \bar{v}_{gd}(t_k)) \tag{2.10}$$

Now, to calculate the two-sample deadbeat law (predictive) let $i_d(t_{k+2}) = i_{ref}(t_k)$ and by applied an advance of sampling period in equation (2.10).

$$v_o(k) = \frac{L_n}{L}[i_{ref}(t_k) - i_d(t_{k+1})] + \bar{v}_{gd}(t_{k+1}) \tag{2.11}$$

Equation (2.11) observes we want to find the prediction value of $\bar{v}_{gd}(t_{k+1})$ for four successive achievements of $\bar{v}_{gd}(t_k)$.

$$\bar{v}_{gd}(t_{k+2}) - \bar{v}_{gd}(t_{k+1}) = \bar{v}_{gd}(t_{k+1}) - \bar{v}_{gd}(t_k) \tag{2.12}$$

Therefore:

$$\bar{v}_{gd}(t_{k+1}) = \frac{5}{2}\bar{v}_{gd}(t_k) - \frac{3}{2}\bar{v}_{gd}(t_{k-1}) \tag{2.13}$$

Also the harmonics in the grid voltage can be eliminated by inserting an output filter, so the transfer function of the close loop shown in Figure (2.3) can be expressed as;

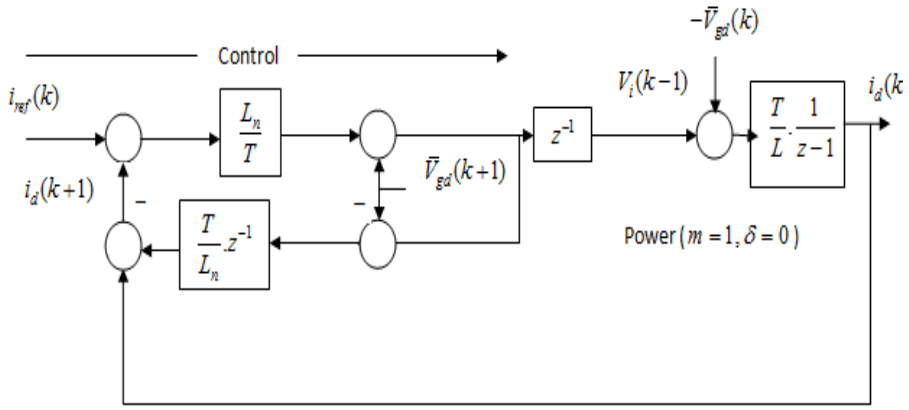

Figure 2.3: Block Diagram of PC [9]

$$H(z) = \frac{L_n}{L}.\frac{1}{(z-1)(z+1)} \tag{2.14}$$

2.2.2 Robust Predictive Current Control (RPCC)

It uses to achieve the same task when we use the two-sample deadbeat control law [9], here we investigate the 'Luenberger observer' to calculate the future value of the current.

$$i_d(t_{k+1}) = (1-k_o).\bar{i}_d(t_k) + k_o.\hat{i}_d(t_k) + \frac{T_s}{L_n}(v_i(t_{k-1}) - \bar{v}_{gd}(t_k)) \tag{2.15}$$

We can evaluate the convergence speed of the estimation by the observer pole $(z = 1 - k_0)$, where k_0 is the observer gain, $k_0 \in [0,1]$.

In particular case $k_0 \to 1$, there are two types of RPCC.

2.2.3 RPCC with Sampling before the Calculation Interval

$$H(z) = \frac{k_o L_n}{L} . \frac{1}{(z-1)(z+k_o)} \tag{2.16}$$

$$PM = \frac{\pi}{2} - 2\arctan\left(\frac{k_o / 2}{1+k_o}\right) - \arctan\left(\frac{k_o(1-k_o)}{2(1+k_o)^2}\right) \tag{2.17}$$

$$GM(in\ decibels) = 20.\log\left(\frac{1+k_o}{k_o}\right) \tag{2.18}$$

In general, the RPCC significantly increases the stability margins of the normal predictive controllers and the phase margin can be improved even more by sampling during the computation interval.

2.2.3.1 RPCC with Sampling during the Calculation Interval

Here we $\varepsilon \neq 0$, considering the stability condition.

$$\varepsilon > \frac{3}{2} - \frac{1}{k_o} \tag{2.19}$$

$$H(z) = \frac{k_o L_n}{L} . \frac{(1-\varepsilon)z + \varepsilon}{(z-1)(z+k_o)} \tag{2.20}$$

If $k_o \geq \frac{2}{3}$ RPCC is unstable. But, if $k_o < \frac{2}{3}$ the RPCC is be stable at any value of t_d in [0,2T].

$$GM = \left(\frac{L_n}{L}\right)_{\max} \tag{2.21}$$

If $k_o = 0.5$ and $\varepsilon = 0.5$, then the limit is L_n = 6L and PM = 77°

$$PM = \frac{\pi}{2} - 2\arctan\left(\frac{k_o/2}{1+k_o}\right) - \arctan\left(\frac{k_o(1-k_o)}{2(1+k_o)^2}\right) + \arctan\left(\frac{k_o(1-k_o)}{1+k_o}\right) \qquad (2.22)$$

2.3 Adaptive Dead-Time Compensation

This types of current control strategy uses a new software-based plug-in dead-time compensator for grid–connected pulse width modulated voltage source inverters of single-stage photovoltaic (PV) systems using predictive current controllers (PCCs) to regulate phase current. First, a nonlinear dead-time disturbance model which is used for the generation of a feed-forward compensation clamping effects around zero-current crossing points. A novel closed-loop adaptive adjustment scheme is proposed for fine tuning in real time of the compensation model parameters, thereby ensuring results even under the highly varying operating conditions typically found in PV system due to insulation temperature, and shadowing effects, among other. The algorithm implementation is straightforward and computationally efficient, and can be easily attached to an existent PCC to enhance its dead-time rejection capability [16].

Phase currents generated by the CC-VSI must satisfy strict harmonic limits of currnet quality standards even under severe grid voltage distortion and unbalances. With the increasing penetration of distributed power generation units, additional features are being required, such as reactive power injection, fault ride-through capabilities, and compensation of harmonic currents generated by nearly nonlinear loads.

To meet all of the previous requirements, the current controller becomes a key part of the system. In this context, PCC is a very attractive solution due to its robustness against

plant mismatch, implementation simplicity, and low computation cost, compared to other controls, such as proportional-integral (PI) or proportional resonant controllers. PCCs tolerate large parameter variations without incurring instability and with a marginal, decrease of its tracking accuracy. Also, shorts on the grid terminals can be quickly compensated without current overshoots [17].

In this thesis I consider a new control method based on a disturbance estimator for a three-phase grid-connected inverter. The various components that deteriorate the performance of a conventional PCC are regarded as disturbances, and a disturbance estimator is constructed using an inverter output voltage and current values. Moreover, the grid angle is extracted by using phase locked loop (PLL) with estimated reactive component of disturbance. Furthermore, we limited the system gains corresponding with the grid balance conditions.

Chapter 3

MODELING OF THREE PHASE INVERTER

In this chapter, we see the standard form of 'three-phase half bridge inverters' that forms the important part which connects the DC sources represented by the renewable energy to a load, which may be a normal load or the grid.

The inverter consists of six IGBT transistors which act as electronic switches. The collector terminals of the upper transistors shown in Figure (3.1) are connected to the DC source's positive terminal and emitters are connected to the collector terminals of the lower transistors. The emitters of the lower transistors are connected to the DC source's negative terminal. Third terminal is the control terminal called the gate.

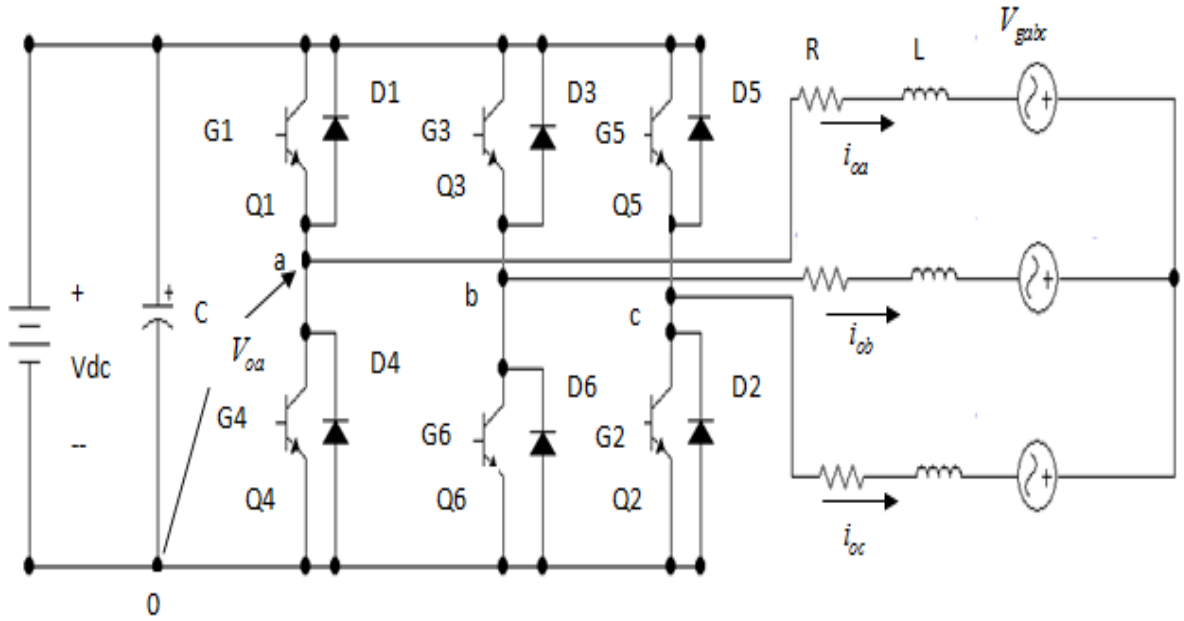

Figure 3.1: Three Phase Grid-Connected Inverter [20]

There are two popular types of inverters with respect to the output voltage waveform: square wave (SW) and Pulse width modulation (PWM). The last one is preferred to the first one because PWM techniques produce less harmonics than the SW and the output voltage is an approximation to the sinusoidal waveform.

Figure 3.1 shows the structure of the three-phase inverter connected to the three-phase grid via an R-L filter. The general three-phase system equations in *abc* sequence can be written as follows:

The output phase voltages;

$$V_{oa} = R.i_a + L.\frac{di_a}{dt} + V_{ga} \tag{3.1}$$

$$V_{ob} = R.i_b + L.\frac{di_b}{dt} + V_{gb} \tag{3.2}$$

$$V_{oc} = R.i_c + L.\frac{di_c}{dt} + V_{gc} \tag{3.3}$$

The output line currents;

$$i_{oa} = I_m \cos wt \tag{3.4}$$

$$i_{ob} = I_m \cos(wt - \frac{2\pi}{3}) \tag{3.5}$$

$$i_{oc} = I_m \cos(wt + \frac{2\pi}{3}) \tag{3.6}$$

These equations consider the standard three-phase output for all system generation coming from the normal stator winding of generators which depend for operation on the natural sources, such as oil, natural gas, coal etc., in addition to the power obtained from the clean technology. To make these equations easier to understand requires the use a new transformation, called park transformation that transfers the sequence system from abc to $\alpha\beta$ or dq .We implement the new system model by using space vector PWM techniques.

3.1 Space Vector Pulse Width Modulation (SVPWM)

This is an advanced method for PWM techniques. It has the ability that puts it in the first of control methods and is the best when we demand a variable frequency drive application with high performance characteristics [2]. SVPWM would be used for the control circuit of the power inverter if simplicity and high accuracy are required. In this method we have eight states of space-vectors, six of them are active and two zero vectors represent the reference vectors (reference voltage) shown in Figure 3.2. Table 3.1 gives a summary of the switching states and all values of the phase voltages.

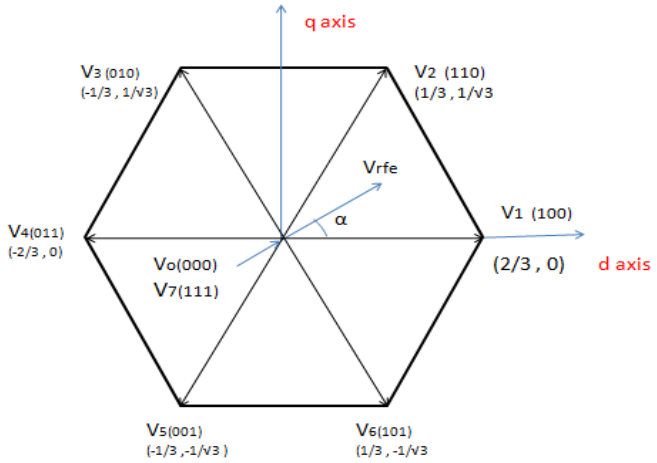

Figure 3.2: Basic Switching Vectors and Sectors [2]

Table 3.1: Switching States and Output Voltage [19]

State	On devices	V_{oa}	V_{ob}	V_{oc}	Space voltage vector
0	$Q_4Q_6Q_2$	0	0	0	$\bar{V}_0(000)$
1	$Q_1Q_6Q_2$	$\frac{2V_{dc}}{3}$	$\frac{-V_{dc}}{3}$	$\frac{-V_{dc}}{3}$	$\bar{V}_1(100)$
2	$Q_1Q_3Q_2$	$\frac{V_{dc}}{3}$	$\frac{V_{dc}}{3}$	$\frac{-2V_{dc}}{3}$	$\bar{V}_2(110)$
3	$Q_4Q_3Q_2$	$\frac{-V_{dc}}{3}$	$\frac{2V_{dc}}{3}$	$\frac{-V_{dc}}{3}$	$\bar{V}_3(010)$
4	$Q_4Q_3Q_5$	$\frac{-2V_{dc}}{3}$	$\frac{V_{dc}}{3}$	$\frac{V_{dc}}{3}$	$\bar{V}_4(011)$
5	$Q_4Q_6Q_5$	$\frac{-V_{dc}}{3}$	$\frac{-V_{dc}}{3}$	$\frac{2V_{dc}}{3}$	$\bar{V}_5(001)$
6	$Q_1Q_6Q_5$	$\frac{V_{dc}}{3}$	$\frac{-2V_{dc}}{3}$	$\frac{V_{dc}}{3}$	$\bar{V}_6(101)$
7	$Q_1Q_3Q_5$	0	0	0	$\bar{V}_7(111)$

Now for implementation, firstly we transfer the abc equations to $\alpha\beta$ stationary reference frame; after that we transfer from the $\alpha\beta$ to dq synchronous reference frame, in which the current controller is realized. It becomes easier to represent all the system equations by two orthogonal components. This strategy is known as (SVM).

Space vector voltage equation;

$$V_o = \frac{2}{3}(V_{oa} + aV_{ob} + a^2V_{oc}) \tag{3.7}$$

$$i_o = \frac{2}{3}(i_a + ai_b + a^2i_c) \tag{3.8}$$

By substituting equations [(3.4),(3.5),(3.6)], in (3.8) we obtain the two orthogonal components; one is the real part called i_α and the other one is imaginary called i_β.

Using the complex quantities $a = e^{j\frac{2\pi}{3}}$ and $a^2 = e^{j\frac{4\pi}{3}}$ we get

$$i_{o\alpha} = I_m \cos wt \tag{3.9}$$

$$i_{o\beta} = jI_m \sin wt \tag{3.10}$$

Therefore, the output current becomes $i_o = I_m e^{jwt}$. Here the phase shift equals zero. The most important thing that the inductive load represents the greater percentage of the types of load demands, therefore, the output voltage is always leading by angle φ known as the power factor angle. Then;

$$V_o = V_m e^{j(wt+\varphi)} \tag{3.11}$$

Also, we can write the voltage and current not only in stationary reference frame but in the dq synchronous reference frame by using the rotational transformation e^{-jwt} .

$$V_{o(dq)} = V_o e^{-jwt} = V_m e^{j\varphi} = V_{od} + V_{oq} \tag{3.12}$$

$$i_{o(dq)} = i_o e^{-jwt} = I_m \tag{3.13}$$

Now, when all these transformations are applied to our model in Fig. 3.1 we obtain

$$V_o = R.i_o + L.\frac{di_o}{dt} + V_g \tag{3.14}$$

$$V_{o(dq)} = R.i_{o(dq)} + jwL.i_{o(dq)} + L\frac{di_{o(dq)}}{dt} + V_{g(dq)} \tag{3.15}$$

Equation (3.15) demonstrates the system model which will be used in the formulation of the closed-loop control system. But this equation cannot be considered to be exactly representing the actual system, since the system dynamics usually have diverse uncertainties. For instance, parameter variations, grid voltage disturbances involving low order harmonic and unbalanced conditions, then require to be more careful during controller design.

In this case we use the nominal parameter values and considering those uncertainties as dynamic disturbances. Then (3.15) can be written as.

$$V_{odq}(t_k) = R_n.i_{dq}(t_k) + jwL_n.i_{dq}(t_k) + L_n\frac{di_{dq}(t_k)}{dt} + f_{dq}(t_k) \tag{3.16}$$

$$f_{dq} = \Delta R.i_{dq} + jw\Delta L.i_{dq} + \Delta L\frac{di_{dq}}{dt} + v_{gdq} + u_{dq} \tag{3.17}$$

Where $L = L_n + \Delta L$, $R = R_n + \Delta R$, and u_{dq} denotes the disturbances resulting from the low order harmonics and unbalanced grid conditions [20].

Moreover, there are several requirements related to the base issue of inverter design. Table 3.2 observes the date which we have been used in the simulation program.

Chapter 4

CURRENT CONTROL STRATEGY

In this chapter we will demonstrate how we can investigate the digital implementation of the current controller (CC) by using digital signal processor (DSP) microcontroller [21], [22]. This technique is considered the best compared with the other method which use a proportional-integral (PI) controller. The proposed predictive controller (PC) has properties that enable it to predict and track the system in the future steps, which gives it the ability to control the desired variable, and provide a satisfactory dynamic response.

4.1 Discrete time

'ADC' is commonly used with any digital system when the input signal is continuous-time, like the electrical voltage and current. ADC has important role to make the control delay very small by setting the sampling frequency to two times the time delay needed to predict when the inverter is connected with to the grid. The simple diagram shown in Figure 4.1 observes this method.

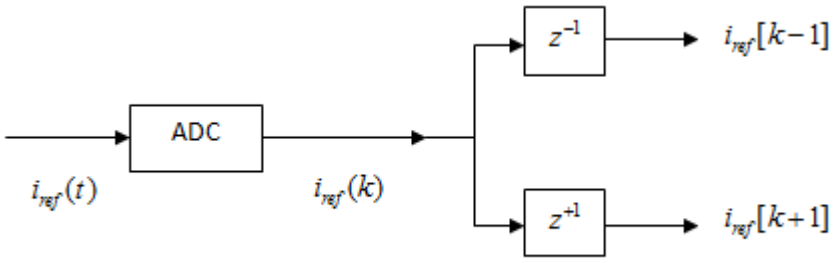

Figure 4.1: Block Diagram Description of Continuous Time Converting to Discrete Time

4.2 Predictive Current Control (PCC)

In chapter three we demonstrated the dynamic equations related to the proposed model. In this chapter we will constrain our care to the digital implementation. Starting from equation (3.16) for the (dq) control voltage, discrete-time domain of the derivative current can be represented by forward numerical approximation as follows.

$$\left(\frac{di_{dq}}{dt}\right)_{t_k} = \frac{i_{dq}(t_{k+1}) - i_{dq}(t_k)}{T_s} \tag{4.1}$$

$$V_{odq}(t_k) = R_n.i_{dq}(t_k) + jwL_n.i_{dq}(t_k) + L_n.\frac{i_{dq}(t_{k+1}) - i_{dq}(t_k)}{T_s} + f_{dq}(t_k) \tag{4.2}$$

In general the method used in the digital current control is usually the traditional technique named asymmetrical PWM shown in figure 4.2. The inverter output voltage in equation 4.2 is generated at sample time t_k, and in the same sequence the grid voltage $V_{gdq}(t_k)$ and the inverter output current $i_{dq}(t_k)$ are sampled. Subsequently, the demanded control algorithms, for example grid synchronization and current control which reduces the current error, are achieved in one sampling period. Then, we calculate the updated value of $v_{gdq}(t_{k+1})$ which represents the inverter output voltage generated at sample time t_{k+1}. In figure 4.2 we assume that the reference current does not change $i^*_{dq}(t_k) = i^*_{dq}(t_{k+1}) = i^*_{dq}(t_{k+2})$). After t_{k+2} the actual current reaches to the desired current in order to enhance the current response with delay time compensation. In this case the output inverter current is tracking the desired current. Moreover, the DC input inverter

voltage must be large enough to guard against any sudden disturbance which could lead the inverter to exit out of the system operation.

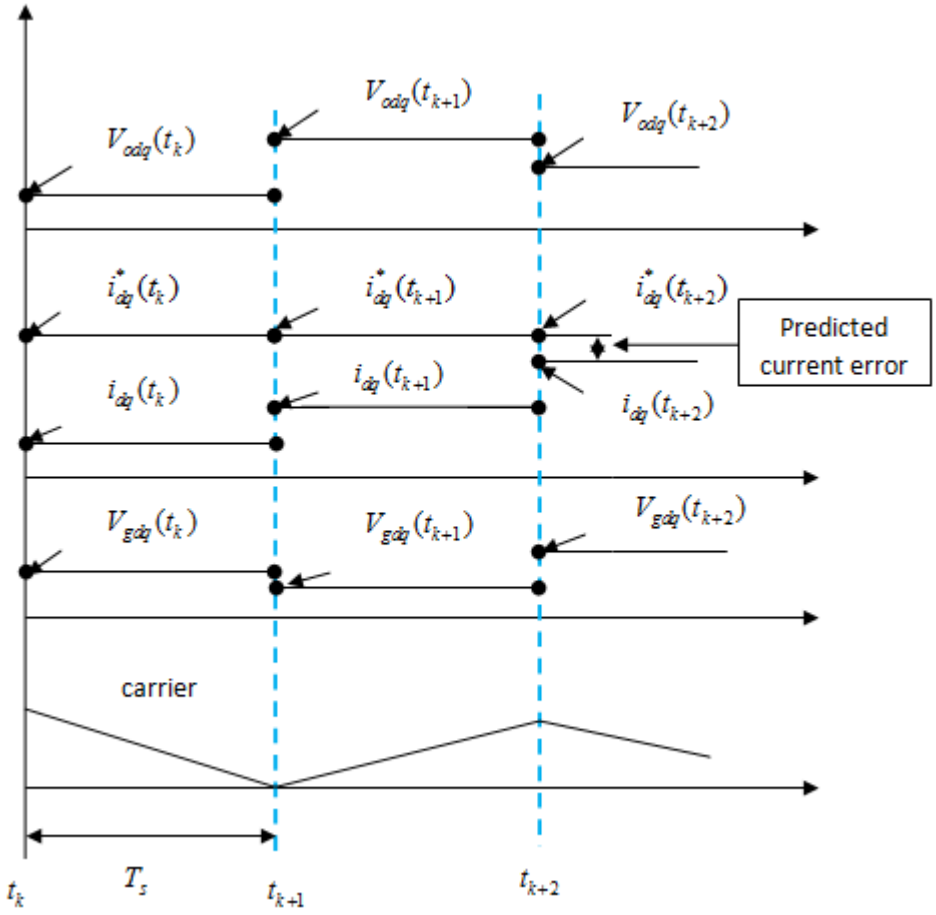

Figure 4.2: Time Sequence of the Digital Current Control [20]

From equation (4.2) we can find the (PC) at discrete time t_{k+1}

$$i_{dq}(t_{k+1}) = i_{dq}(t_k) - \frac{T_s R}{L} i_{dq}(t_k) + \frac{T_s}{L}\left(V_{odq}(t_k) - V_{gdq}(t_k)\right) \tag{4.3}$$

Equation (4.3) represents the inverter output current at steady state since the disturbance values approach to zero($\Delta L = 0, \Delta R = 0$), and represented by only the grid voltage.

By using SVPWM to illustrate the above explanation, we select sector (N=1), $V_1 = (2/3)V_{d.c}$, $V_2 = ((1/3) + j(1/\sqrt{3}))V_{dc}$. Each of these two vectors has two components (real and imaginary parts), so the current also has two components: i_d real current, and i_q imaginary current and each two vectors separated by angle known α (space vector angles). In Figure (4.3) we show all these details.

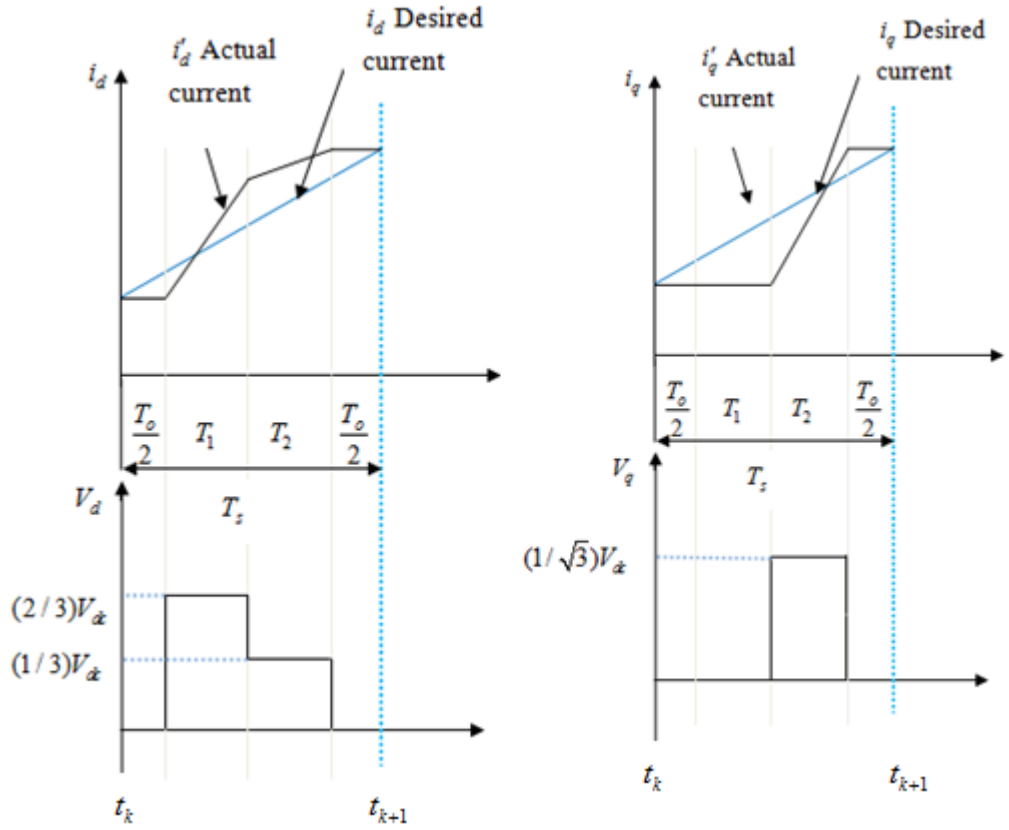

Figure 4.3: Desired and Actual Current with Sequence Voltage in Ts (d and q axis quantities in sector 1) [23]

There are four instantaneous values of the actual current in the sampling interval of duration T_s, which can be written as follows.

In $0 \le t_p < t_{k+T_o/2}$

$$i_1 = i_{dq}(t_{k+T_o/2}) = i_{dq}(t_k)\left(1-\frac{RT_o}{2L}\right)+\frac{T_o}{2L}(-V_{gdq}(t_k)) \tag{4.4}$$

Note: In this interval the value of $V_{odq}(t_k) = 0$.

$$i_2 = i_{dq}(t_{k+(T_o/2)+T_1}) = i_{dq}(t_{k+(T_{o/2})})\left(1-\frac{RT_1}{L}\right)+\frac{T_1}{L}(V_k - V_{gdq}(t_k)) \tag{4.5}$$

$$i_3 = i_{dq}(t_{k+(T_o/2)+T_1+T_2}) = i_{dq}(t_{k+(T_{o/2})+T_1})\left(1-\frac{RT_2}{L}\right)+\frac{T_2}{L}(V_{k+1} - V_{gdq}(t_k)) \tag{4.6}$$

$$i_4 = i_{dq}(t_{k+1}) = i_{dq}(t_{k+(T_{o/2})+T_1+T_2})\left(1-\frac{RT_o}{2L}\right)+\frac{T_o}{2L}(-V_{gdq}(t_k)) \tag{4.7}$$

Moreover, the time intervals should be evaluated such that the current matches its reference at the end of the sampling interval.

$T_s = 1/f_s$

$$T_1 = M \times T_s \times \sin(\pi/3 - \alpha) \tag{4.8}$$

$$T_2 = M \times T_s \times \sin(\alpha) \tag{4.9}$$

$$\alpha = \tan^{-1}\left(\frac{V_q}{V_d}\right) \tag{4.10}$$

$$M = \sqrt{3} \times \left|V_{odq}(t_k)\right| / V_{dc} \tag{4.11}$$

$$V_k = (2/3) \times V_{dc} \times e^{j(N-1)\pi/3} \tag{4.12}$$

$$V_{k+1} = V_k \times e^{j\pi/3} \tag{4.13}$$

M : Modulation index (0 <M<1) , N: number of sectors

$$T_s = T_o + T_1 + T_2 \Rightarrow T_o = T_s - (T_1 + T_2) \tag{4.14}$$

In order to build the PCC which compensates for the above-mentioned time delay, where the current is updated at the sampling instant shifted by one step $i_{k+2} = i^*_{k+2}$, the output control voltage in equation (4.2) becomes

$$V_{odq}(t_{k+1}) = R_n.\hat{i}_{dq}(t_{k+1}) + jwL_n.i_{dq}(t_{k+1}) + L_n.\frac{i^*_{dq}(t_{k+2}) - i_{dq}(t_{k+1})}{T_s} + \hat{f}_{dq}(t_{k+1}) \qquad (4.15)$$

Equation (4.15) is very important since it considers the closed-loop voltage control and we will use it to obtain all the system requirements, for instance the predictive current, estimation angle and system stability.

4.2.1 Disturbance Estimation

Is necessary for the PCC to operate normally, moreover, the dynamic response of the inverter system is affected by the disturbance algorithm used.

On the other hand, the grid voltage component is the more effective component between all of the other disturbance components. A suitably designed estimator can eliminate grid voltage sensors. In this thesis the disturbance estimator is structured in the *dq* synchronous reference frame and depends on the reactive component of the disturbance. We will extract the grid angle by using the phase-locked- loop (PLL) principle.

From equation (4.2)

$$i_{dq}(t_{k+1}) = \left[1 - \frac{T_s}{L_n}(R_n + jwL_n)\right].i_{dq}(t_k) + \frac{T_s}{L_n}\left(V_{odq}(t_k) - f_{dq}(t_k)\right) \qquad (4.16)$$

Assuming that, $f(t_k) = f(t_{k+1})$. State Space Equation [20] can be obtained as follows;

$$x(k+1) = Ax(k) + b.V_{odq}(k) \quad , t_k = k \qquad (4.17)$$

$$x(k+1)=\begin{bmatrix} i_{dq}(t_{k+1}) \\ f_{dq}(t_{k+1}) \end{bmatrix} \tag{4.18}$$

$$\begin{bmatrix} i_{dq}(t_{k+1}) \\ f_{dq}(t_{k+1}) \end{bmatrix}=\begin{bmatrix} 1-T_s(R_n+jwL_n)/L_n & -T_s/L_n \\ 0 & 1 \end{bmatrix}\begin{bmatrix} i_{dq}(t_k) \\ f_{dq}(t_k) \end{bmatrix} + \begin{bmatrix} T_s/L_n \\ 0 \end{bmatrix} V_{odq}(t_k) \tag{4.19}$$

The desired estimator has the form in equation (4.20), where G is a gain matrix, and $\Delta x(k)$ represents the difference between the actual value and the estimation value;

$$\hat{x}(k+1)=A\hat{x}(k)+b.V_{odq}(k)+G\Delta x(k) \tag{4.20}$$

According to (4.18) the estimator equations can be written explicitly as

$$\begin{bmatrix} \hat{i}_{dq}(t_{k+1}) \\ \hat{f}_{dq}(t_{k+1}) \end{bmatrix}=\begin{bmatrix} 1-T_s(R_n+jwL_n)/L_n & -T_s/L_n \\ 0 & 1 \end{bmatrix}\begin{bmatrix} \hat{i}_{dq}(t_k) \\ \hat{f}_{dq}(t_k) \end{bmatrix} + \begin{bmatrix} T_s/L_n \\ 0 \end{bmatrix} V_{odq}(t_k)+\begin{bmatrix} l_1 \\ l_2 \end{bmatrix}\times \left(i_{dq}(t_k)-[1\ \ 0]\begin{bmatrix} \hat{i}_{dq}(t_k) \\ \hat{f}_{dq}(t_k) \end{bmatrix}\right) \tag{4.21}$$

Where (l_1, l_2) represent the estimator closed-loop gains which can easily be found by using the pole placement method [24].

From (4.21) we can write explicitly.

$$\hat{i}_{dq}(t_{k+1})=[1-T_s/L_n(R_n+jwL_n)]\hat{i}_{dq}(t_k)+T_s/L_n(V_{odq}(t_k) - \hat{f}_{dq}(t_k))+l_1\Delta i_{dq}(t_k) \tag{4.22}$$

and

$$\hat{f}_{dq}(t_{k+1})=\hat{f}_{dq}(t_k)+l_2\Delta i_{dq}(t_k) \tag{4.23}$$

The disturbance estimator in the discrete-time domain can be explicitly depicted in the block diagram shown in figure 4.4. It consists of two inputs $i_{dq}(t_k)$ and $V_{odq}(t_k)$, which represent the inverter output current and voltage input to the disturbance estimator system, and the output variables are the current estimation $\hat{i}_{dq}(t_k)$, and the disturbance estimation $\hat{f}_{dq}(t_k)$. These estimation output values are very important when we want to estimate the grid angle and in stability analysis, which we will discuss later.

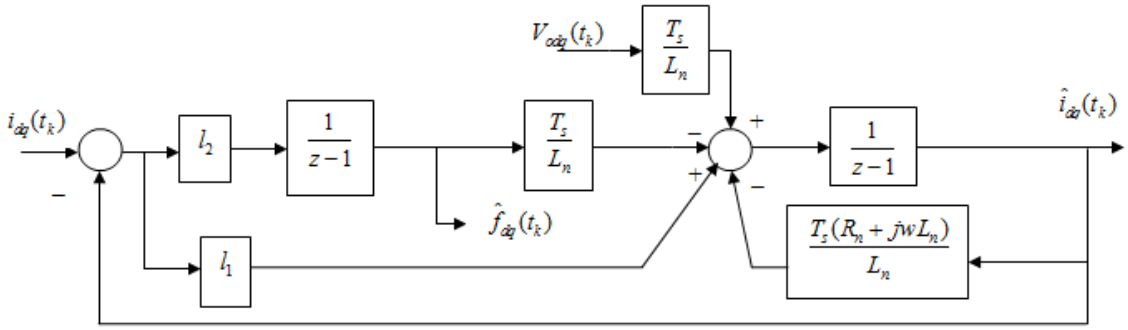

Figure 4.4: Disturbance Estimator in Discrete-Time Domain [20]

4.2.2 Phase Locked Loop (PLL) For Frequency Synchronization

Synchronization is more used in power generation and conversion when we have normal generator power system or when we have voltage source inverter. we mean that the frequency must be constant at 50 Hz or 60 Hz. In a synchronous machine, the speed of the rotor rotation is the same as that of the magnetic field (flux), which corresponds to synchronous frequency. PLL is not used in power systems field only, but it is also used in communication and radar systems to match between the signals transmission and receiving. The growing demand for electrical power calls for the need to use renewable energy for the purpose of the shortfall in the compensation network grid. Therefore, the use of PLL is necessary in a grid-connected inverter to estimate the angular frequency

$\hat{w}$ that is considered one of the important requirements that enters in the closed loop voltage control calculation [25].

The input value applied to PLL system comes from the disturbance estimation system shown in Figure 4.4, which means the PLL is designed to work with the dq frame. We considered only the reactive component of the disturbance estimator $\hat{f}_q(t_k)$. Figure 4.5 shows the block diagram of PLL, consisting of two stages: first is the PI controller that is used to produce the suitable change in the angular frequency (Δw) which has the ability to track the instantaneous changes in phase angle [26]. The output of PI is added with the constant reference angular frequency $w^*(t_k)$, that gives $\hat{w}(t_k)$ is the estimated angular frequency.

$$\hat{w} = \frac{d\hat{\theta}}{dt} \tag{4.24}$$

Second stage is the discrete-time integration circuit that produces the angle estimate from the angular frequency. PLL bandwidth is chosen as 100Hz. This gives robust performance with the system variation.

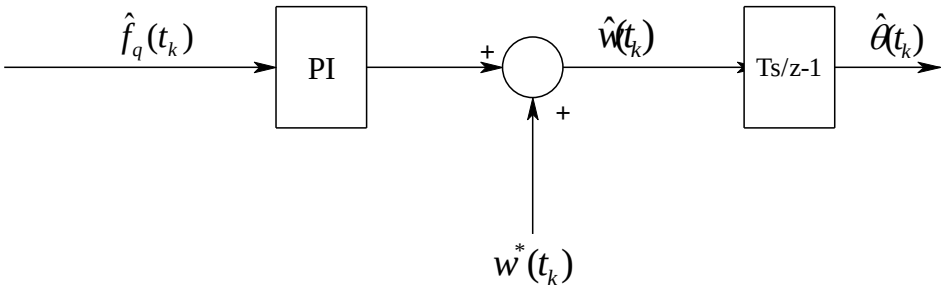

Figure 4.5: PLL Block Diagram [20]

4.2.2.1 PLL Transfer Function

From the block diagram shown in Figure 4.5 we can find the TF which describes the working principle of the PLL circuit. By using Laplace transformation we can express the system as follows.

$$G_{PI} = \left(K_p \frac{1+s\tau}{s\tau} \right) \tag{4.25}$$

$$G_{\text{int}} = \left(\frac{1}{s} \right) \tag{4.26}$$

The input q- component of the disturbance to the PLL is in discrete time domain and the PI-TF should be in discrete time, so the numerical solution going from s-domain to z-domain is as follows.

$$G_{PI}(z) = \frac{w_q(z)}{\hat{f}_q(z)} = K_p \left(\frac{z-1+(T_s/\tau)}{z-1} \right) \tag{4.27}$$

$$G_{\text{int}}(z) = \frac{\hat{\theta}(z)}{\hat{w}(z)} = \left(\frac{T_s}{z-1} \right) \tag{4.28}$$

Note: $s = \frac{z-1}{T_s}$, $k = t_k$, K_p = PI controller gain , τ =time constant $\approx 10T_s$

$$w_q(k+1) = w_q(k) + K_p \hat{f}_q(k+1) - K_p(1-(T_s/\tau))\hat{f}_q(k) \tag{4.29}$$

$$\hat{w}(t_k) = w_q(t_k) + w^*(t_k) \tag{4.30}$$

$$\hat{\theta}(k+1) = \hat{\theta}(k) + T_s \hat{w}(k) \tag{4.31}$$

4.2.3 Lagrange Interpolation

Equation (4.15) includes three unknown values, two of which we will see how can be calculated. First one is the reference current $i_{dq}^*(t_{k+2})$ and the other one is the future one-

step-ahead value of the disturbance estimate $\hat{f}_{dq}(t_{k+1})$. Lagrange interpolation is a suitable method for extrapolating an nth order polynomial. It is useful when we want to obtain the two-step prediction of the reference current or the one-step prediction of the disturbance estimation, by taking advantage of the fact that the sample time is fixed [23].

The general form of the (m^{th}) order prediction is given in the polynomial form shown in equation (4.32).

$$I_p^*(k+1) = \sum_{l=0}^{m} (-1)^{m-l} \binom{m+1}{l} I^*(k+l-m) \tag{4.32}$$

For our problem m=2, giving

$$\hat{f}_{dq}(t_{k+1}) = 3\hat{f}_{dq}(t_k) - 3\hat{f}_{dq}(t_{k-1}) + \hat{f}_{dq}(t_{k-2}) \tag{4.33}$$

Equation (4.33) is for disturbance and equation (4.34) is for reference current. Now the inverter output voltage can be calculated after we substitute equations (4.33), (4.34) in (4.15). The third unknown value is $i_{dq}^*(t_{k+1})$, which also can be easily predicted from equation (4.16)

$$i_{dq}^*(t_{k+2}) = 6i_{dq}^*(t_k) - 8i_{dq}^*(t_{k-1}) + 3i_{dq}^*(t_{k-2}) \tag{4.34}$$

The main advantages and disadvantages of the Lagrange interpolation formula are follows.

Advantages;

Its simplicity facilitates model analysis**.**

It is easy for mathematical applications, for instance differentiation and integration.

Disadvantages;

It may not capture track of data.

Not feasible if data contains a vertical asymptote.

4.3 Stability Analysis

In general stability of electric power systems is one of the first priorities that is taken into consideration when we design the control strategies. Therefore one must focus on all those aspects that may lead to loss of stability. In the classical power system using generators to produce active and reactive power, the system stability is dependent on events which occur in the distribution system, such as sudden changes in load demand or symmetrical or unsymmetrical fault (short circuit) or switching in transmission lines. One of these cases may cause loss of system stability. However, in renewable sources using inverters, we don't have mechanical equipment but we have another main effect coming from the circuit parameter that is used as a filter connecting the inverter and consumers, here for instance a grid. So, with respect to the filter parameter we have two components resistance and inductance. In this case by investigating the influence of the filter parameter disparity on the performance of the disturbance estimator, we will analyze the effect of variation in two nominal values (R_n, L_n) The pole loci give us an idea on the location of system poles on the unit circle, which corresponds to the disturbance situation of changing the values of the parameter. In this case the error in R_n and L_n ranging between the (-65% to 65%) of the actual values of L=3mH when L_n is decreasing from 3mH to 1.05mH, the damping ratio of the disturbance estimator is reduced, the pole loci becomes close to the unit circle, with the estimator gains constant

($l_1 = 1.27,\ l_2 = -20$). When the same situation is repeated when (L_n) increases above the actual value approaching 4.95mH, the pole loci again becomes close to the unit circle. Moreover the damping ratio is also increased above the over damping value ($\xi > 1$) resulting in the settling time becoming very large, with no oscillations.

In addition the effects of the series resistance are not as much, because resistance is independent of frequency, so that R_n error does not noticeably affect the overall stability of the disturbance estimator. We will observe all of the previous explanations in the simulation chapter.

Figure 4.6 shows the block diagram of the predictive current controller combined with the disturbance estimator, $V_{dq}(t_{k+1})$ represents the predictive current controller output which is applied at the beginning of the subsequent sampling period (one sampling period delay). Furthermore, because the method involves the estimation algorithm, that use of grid voltage sensors becomes unnecessary.

The combined system is shown in figure 4.6; we can investigate this system's stability via calculation of the eigenvalues for the state variables $i_{dq}(t_k)$, $\hat{i}_{dq}(t_k)$, $\hat{f}_{dq}(t_k)$, (4.35) considered in the system description form below (see in appendix A to for more detail).

$$\begin{bmatrix} i_{dq}(t_{k+1}) \\ \hat{i}_{dq}(t_{k+1}) \\ \hat{f}_{dq}(t_{k+1}) \end{bmatrix} = \begin{bmatrix} 1-\frac{T_s}{L}(R+jwL) & \frac{T_s}{L}\left(R_n+jwL_n\right)-\frac{L_n}{L} & \frac{T_s}{L} \\ l_1 & -l_1 & 0 \\ l_2 & -l_2 & 1 \end{bmatrix} \begin{bmatrix} i_{dq}(t_k) \\ \hat{i}_{dq}(t_k) \\ \hat{f}_{dq}(t_k) \end{bmatrix} + \begin{bmatrix} L_n/L & -(T_s/L) \\ 1 & 0 \\ 0 & 0 \end{bmatrix} \begin{bmatrix} i^*_{dq}(t_{k+1}) \\ f_{dq}(t_k) \end{bmatrix} \quad (4.35)$$

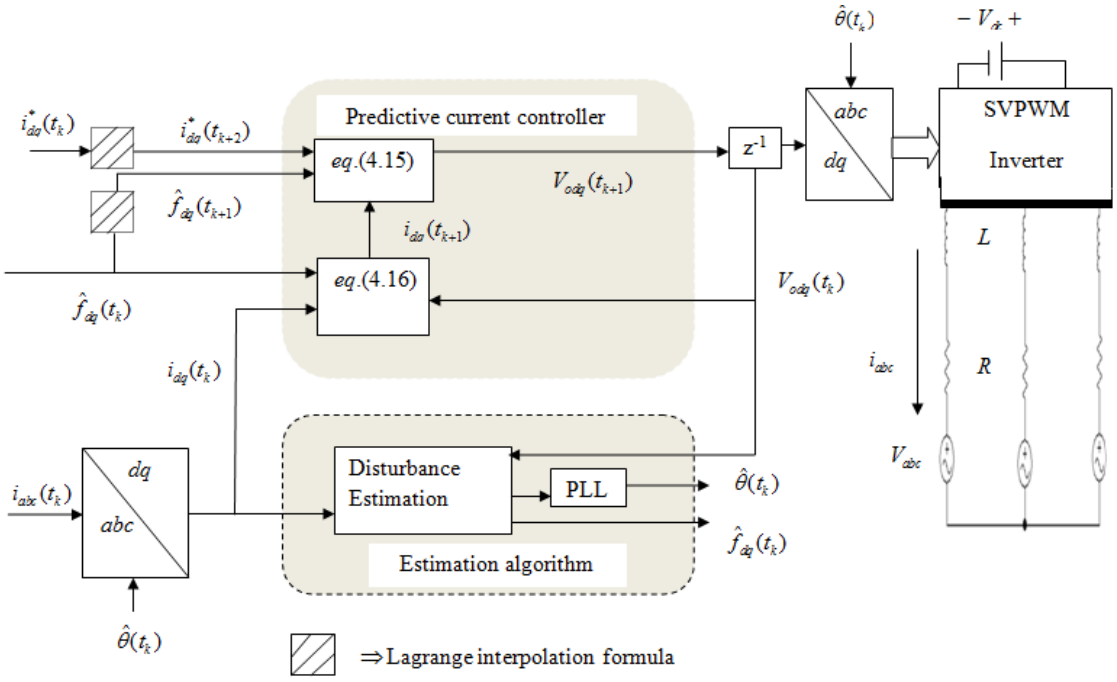

Figure 4.6: Block Diagram for Predictive Current Control [20]

Chapter 5

SIMULATION RESULTS

5.1 Introduction

In this chapter we will see the computer simulation results for the proposed strategy of the predictive current control (PCC) with the description for each programming step. The results are obtained by investigating the disturbance estimator performance, and the specific complex methods used to achieve grid synchronization and system stability without adding sensors to detect the grid voltage. Moreover in the first place by using MATLAB program we obtain the current waveforms in the steady state and for the step change from minimum to maximum and vice versa. Secondly, we will discuss the system synchronization by using PLL techniques and, finally, we investigate the numerical representation to evaluate system stability in discrete-time domain by projection of the poles on the unit circle.

In Table 5.1, the parameters of the system simulated in Matlab-simulink are given.

Table 5. 2: Grid-Connected Inverter's Data

Estimator Gains	l_1	1.27
	l_2	-20
Grid Line-to-Line Voltage		110 Vrms
Grid Frequency		50Hz
DC-I/p Source Voltage		200 V
Filter Inductance		3mH
Equivalent Series Resistance		0.1 Ω
Sampling Frequency		20 KHz
Switching Frequency		10 KHz

5.2 Current Waveforms

The standard three-phase voltage output from any three-phase source consists of three waveforms, having between any two a phase shift of $120°$. The three-phase currents have the same character, but the current shapes depend on the types of the load connection. If the load is a pure resistor the currents and voltages are similar in shape and the phase angle equals zero. However, when the load is not resistive everything changes. In the inverter model we transfer the system analysis from the *abc to dq* then all input values to the (PCC) and the output is in *dq* synchronous reference frame, which is applied to the (SVPWM). So, these two components will have direct effects on the output results of the inverter system. For instance, with high power factor the phase shift between the output currents and voltages is very small. In this case the real

component (d-component) is very large compared with the imaginary component (q-component). Therefore, for any change in reference current (i_d^*) the inverter output currents will have high change; this will be clarified in the next step. On the other hand, the q-component will be considered based on the working of the PLL circuit.

Firstly, Figure 5.1.a demonstrates the steady-state waveforms of the models we proposed in Figure 3.1 grid-connection inverter. We observe the inverter output currents and the grid phase voltage (V_{ga}). In the first step we assume the reference current before prediction is equal to 10A and φ = 0. Figure 5.1.b represents the steady state waveforms of the (d and q) components of the disturbance estimation with the line current (i_{oa}), and the grid angle $\hat{\theta}$ which is estimated by using PLL that observes the synchronization.

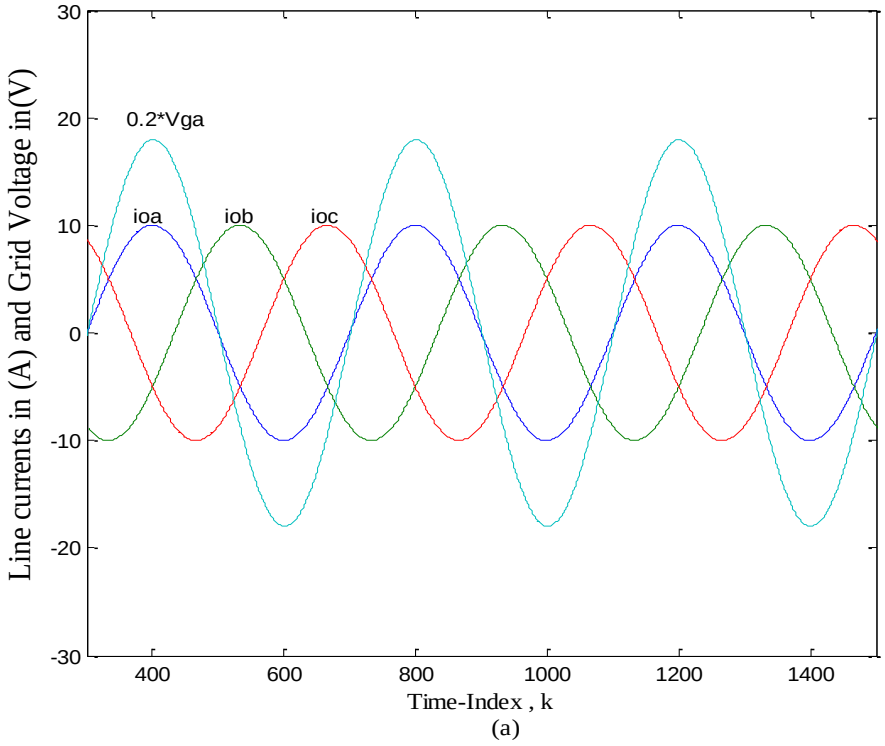

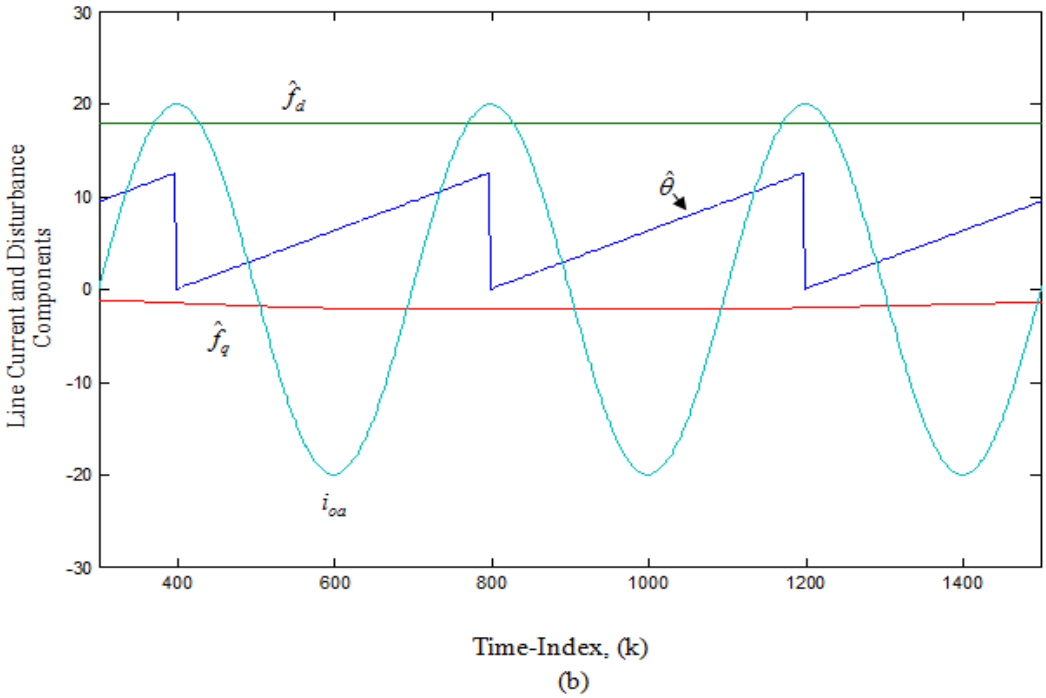

Figure 5.1: Steady State Waveforms (a) Currents and Grid Phase Voltage V_{ga} (b) i_a Scale Multiplied by 2, $\hat{\theta}$ Scale Multiplied by 5, $\hat{f}_d$ Scale Divided by 5 and $\hat{f}_q$ (discrete-time $k = 10^4$ corresponds to t=0.5sec.)

Figure 5.2.a shows the result when we change the reference current from 2 to 10A. In this case we must pay attention to the system stability, because the abrupt change may lead to loss of stability, so we try to make the current increase in the form of a ramp function. We know also that the reference current has two components. The d-component is considered to have more impact when compared with the effect of the q-component. The d-component is greater than the q-component in accordance with the high power factor requirement. In Figure 5.2.b the step change in reference current from 10 to 2 A is shown, where the effect also appears on the ($i_{a,}\ i_{d,}\ i_q\ and\ \hat{\theta}$). We take into account the system stability when the $i_{dq}^{*}(t_k)$ changes from the maximum value 10A to minimum value 2A such that the change must be in the form of a ramp.

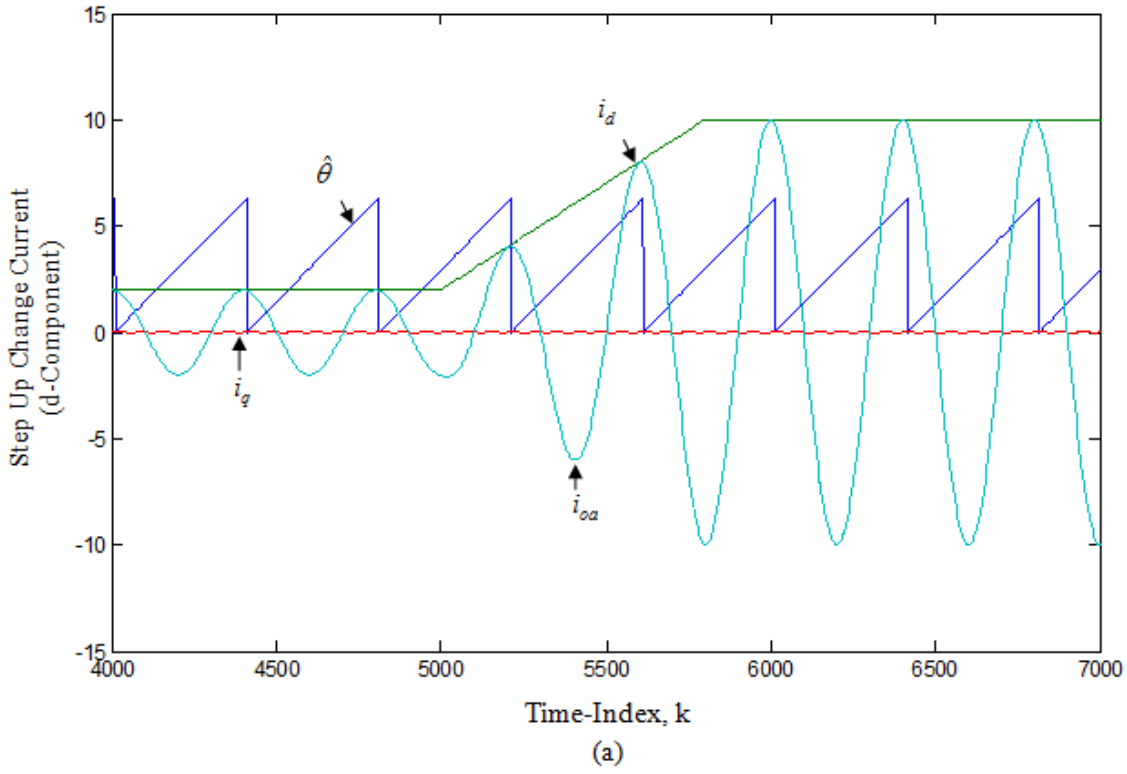

(a)

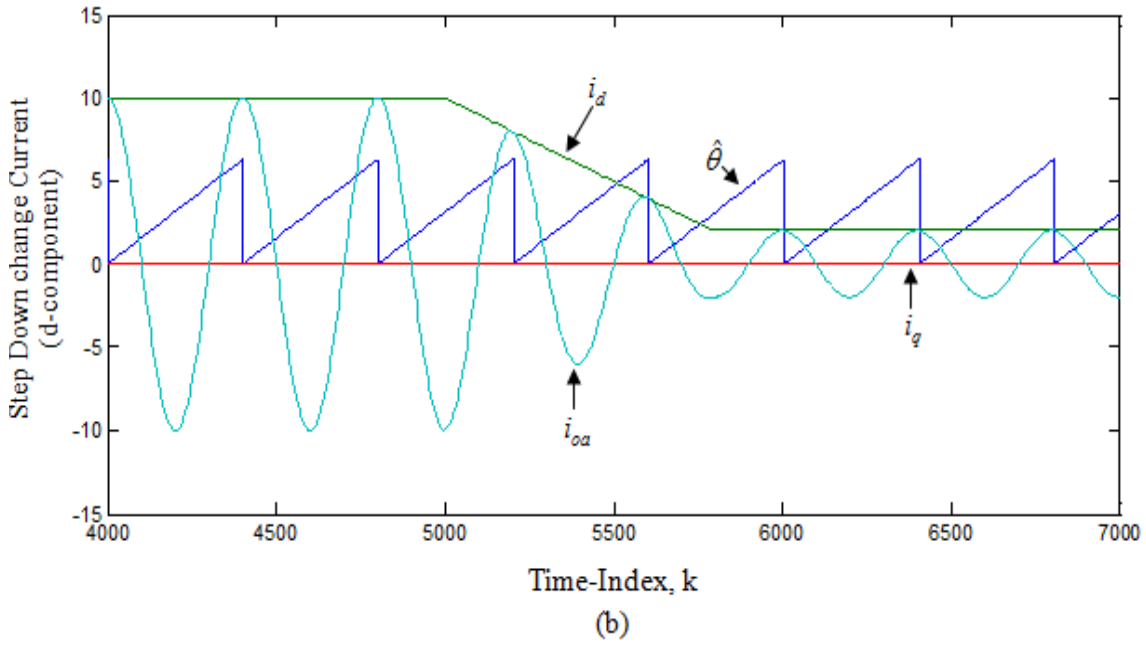

Figure 5.2: Reference Current Step Change and Variations of ($i_{d,}\ i_{q,}\ i_a$ *and* $\hat{\theta}$). (a) Step Change from 2 to 10 A and (b) Step Change from 10 to 2 A (discrete-time $k = 10^4$ corresponds to t= 0.5sec.)

5.3 PLL Waveforms

In this part we use PLL as the standard way to follow in the synchronization of the grid-inverter output to the grid. We shall see that the PLL system is useful and it has high reliability to extract the grid angle. Firstly, we took the imaginary disturbance component (q-component) and enter it to the PI controller to estimate the grid frequency. Figure 5.3.a shows the estimation angular frequency in the steady state. In this case the system operation does not have any change in the reference current, it being equal to the max value 10A. The PI output is summing with the reference angular frequency $w^*(t_k)$ that given as ($\hat{w} = 2\pi F$) which observe in Figure5.3.a.

Notes: Kp represents the proportional gain of the PI; we chose Kp =0.003 that kept the system stable, the integral gain is given by $Ki = \frac{KP}{\tau}$, $\tau = 10T_s$.

Figure 5.3.b shows the angular frequency $\hat{w}$, when the value of the d-component for the reference current is changed from 2 to 10A. This is considered to be a good test for the system synchronization. Moreover, that puts us on the safe side when the change is from the max value to a smaller value, for instance ($10 \rightarrow 2$A).

Figure 5.3.c shows the waveforms of the estimation angle $\hat{\theta}$ which is the output from the integrator. We see that it repeats itself with 2π period, where the standard grid-angle corresponds to the frequency 50Hz.

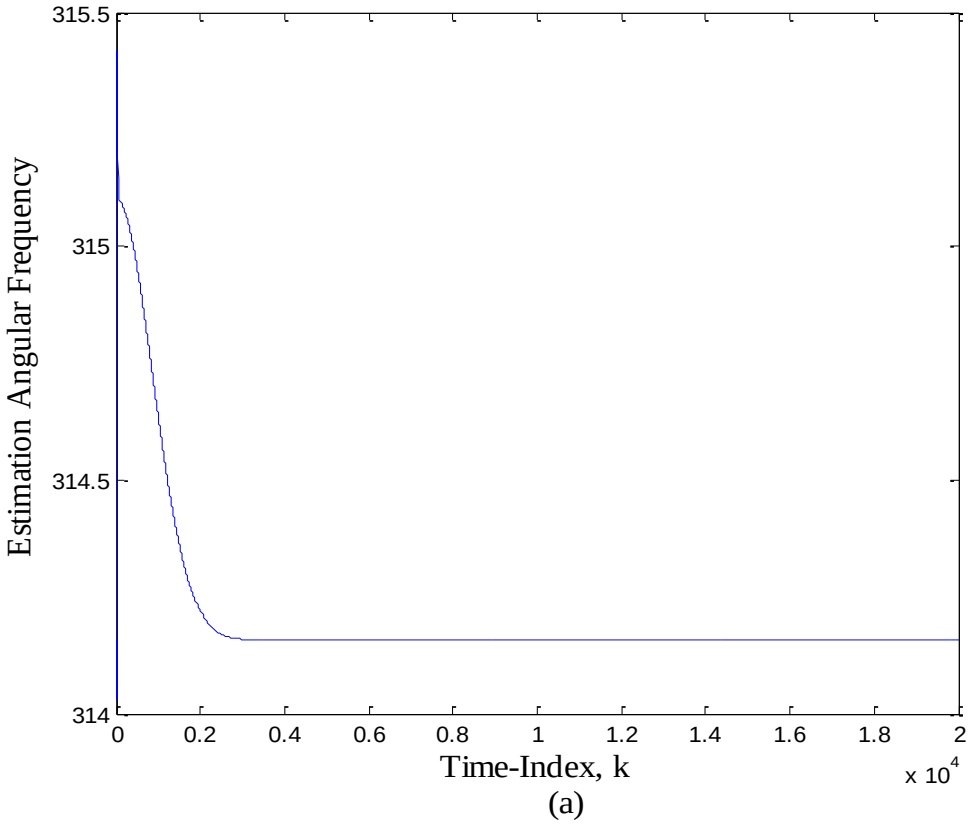
315.5
315
314.5
314
Estimation Angular Frequency
0
0.2
0.4
0.6
0.8
1
1.2
1.4
1.6
1.8
2
Time-Index, k
x 10^4

(a)

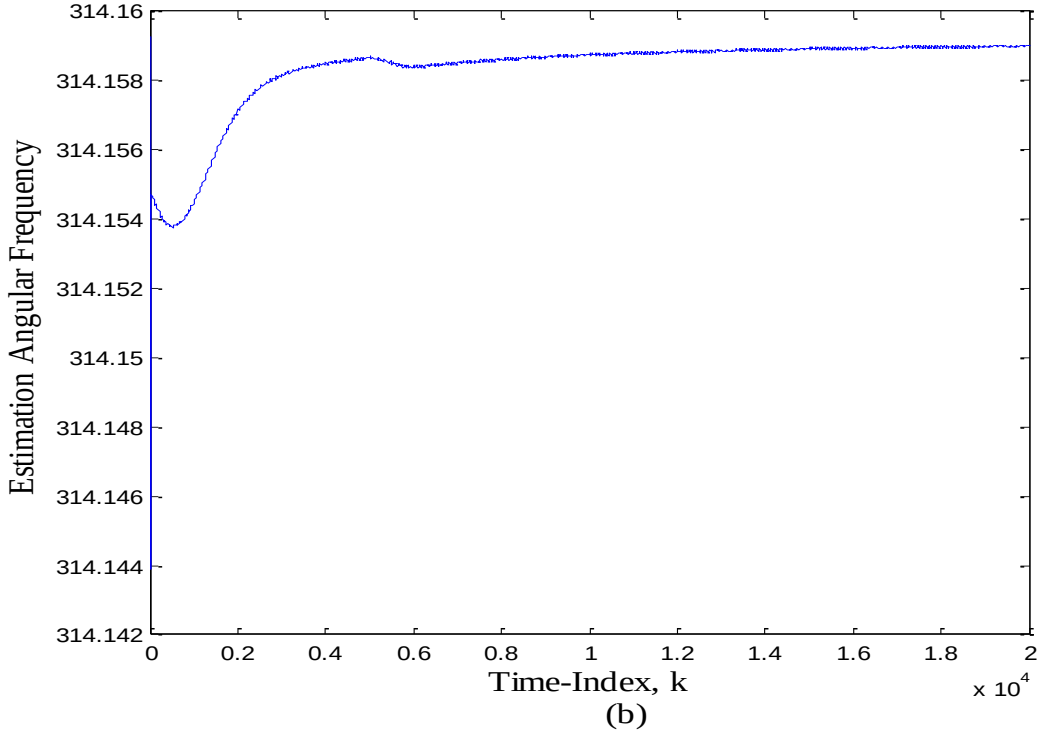
314.16
314.158
314.156
314.154
314.152
314.15
314.148
314.146
314.144
314.142
Estimation Angular Frequency
0
0.2
0.4
0.6
0.8
1
1.2
1.4
1.6
1.8
2
Time-Index, k
x 10^4

(b)

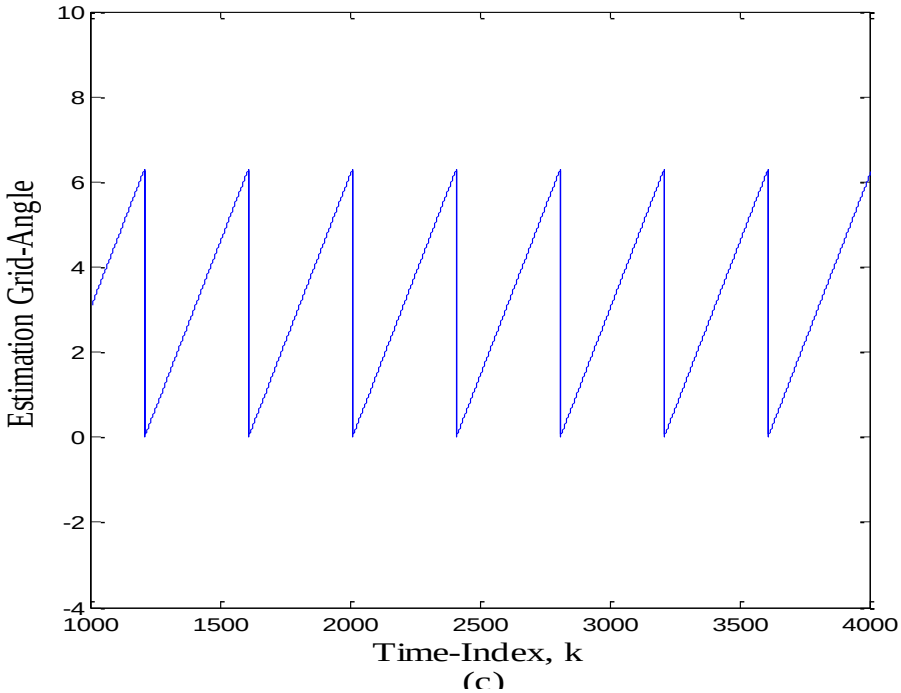

Figure 5.3: PLL Waveforms (a) Estimation of Angular Frequency $\hat{w}$ in Steady State, (b) Estimation of Angular Frequency $\hat{w}$ with Step Change in i_d^* and, (c) Estimation of Grid Angle $\hat{\theta}$ (discrete-time $k = 10^4$ corresponds to t= 0.5sec.)

5.4 Numerical Stability Analysis

One of the most important phenomenons inherent when we speak of any closed-loop system is system stability. In this problem we used numerical analysis to find out when the system is stable and when it becomes unstable. These two cases require from us to select the important parameters that have direct effects. Here we discuss the effects coming from changes in the actual inductance from the nominal value (L_n) when we fix the estimator gains, Also the case when the inductance is fixed at the nominal value and gains are changed is investigated.

5.4.1 Change in the Nominal Inductor (L_n) and Unchanged Gains

From the system matrix in equation 4.34 we calculate the eigenvalues by using MATLAB for different values of Ln from 1.05mH to 4.95mH when the actual value is equal to 3mH and the gains are taken as ($l_1 = 1.27,\ l_2 = -20$). Therefore, we have two cases that we shall discuss as follows.

Stable State;

In this case all the poles are inside the unit circle. Table 5.1 displays the complex eigenvalues computed by the MATLAB program. These values correspond to the poles located inside the unit disc as shown in Figure 5.4. It gives us indication for the system situation, which means that the system is stable according to stability conditions.

Table 5.2: Program Results of Eigenvalues (poles).

L in mH	λ_1	λ_2	λ_3
1.05	-0.8845 - 0.0018i	0.8415 - 0.3892i	0.8477 + 0.3747i
1.35	-0.8005 - 0.0025i	0.8026 - 0.3804i	0.8102 + 0.3665i
1.65	-0.7059 - 0.0033i	0.7597 - 0.3667i	0.7691 + 0.3535i
1.95	-0.5957 - 0.0042i	0.7114 - 0.3460i	0.7228 + 0.3336i
2.55	-0.4585 - 0.0052i	0.5833 - 0.2569i	0.6035 + 0.2465i
2.85	-0.2549 - 0.0067i	0.4586 - 0.0955i	0.5246 + 0.0864i
3.15	0.0205 - 0.3153i	0.0263 + 0.2937i	0.6815 + 0.0059i
3.45	-0.0093 - 0.5177i	0.0007 + 0.4992i	0.7370 + 0.0028i
3.75	-0.0272 - 0.6502i	-0.0153 + 0.6329i	0.7708 + 0.0016i
4.05	-0.0400 - 0.7554i	-0.0266 + 0.7388i	0.7950 + 0.0009i
4.35	-0.0499 - 0.8452i	-0.0353 + 0.8290i	0.8135 + 0.0005i
4.65	-0.0578 - 0.9249i	-0.0423 + 0.9090i	0.8285 + 0.0002i
4.95	-0.0645 - 0.9972i	-0.0480 + 0.9814i	0.8408 + 0.0000i

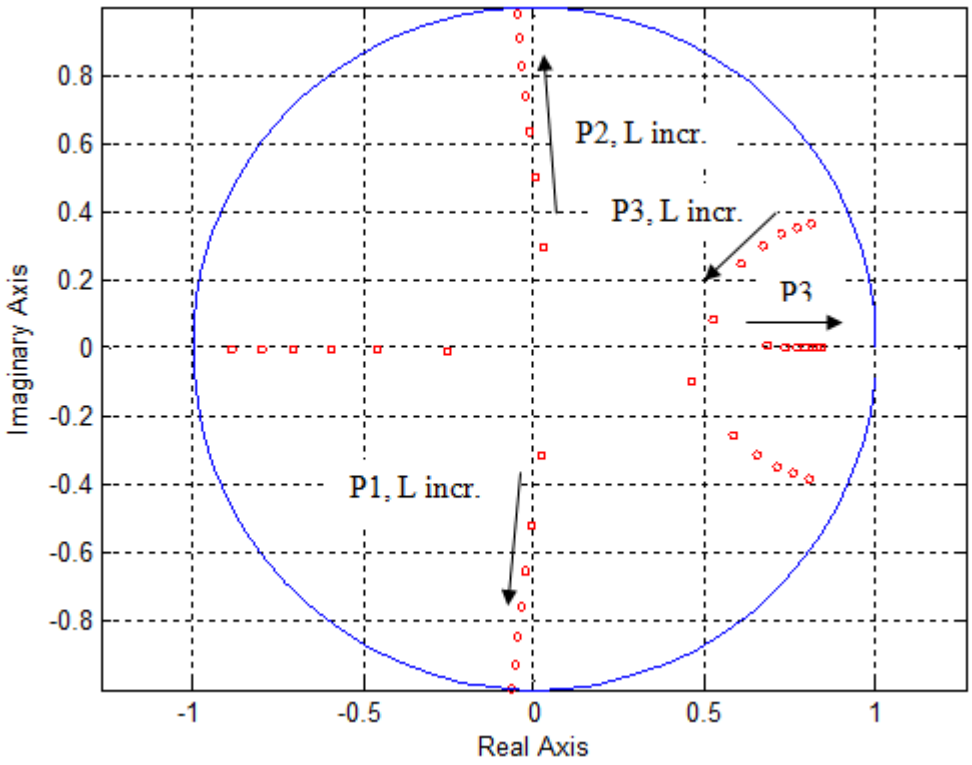

Figure 5.4: Pole Locations of the Disturbance Estimator When L_n Varies from -65% to +65% of the Actual Value (Stable State)

Unstable System

We can say that the system is unstable if one or more of the poles of the closed-loop transfer function go out of the unit circle. This problem occurs when the uncertainty in the inductance value is large. When the values of L_n become greater than 4.95mH or less than 0.78mH causes the system to be unstable. Table 5.2 shows the pole λ_1 from the three poles is out of the unit circle, which is the pole that causes instability. Moreover Figure 5.5.a and Figure 5.5.b depict the two unstable states.

Table 5.3: Program Results of Eigenvalues (poles) at Max and Min of (L_n) Values.

L	λ_1	λ_2	λ_3
Ln Max=5mH	-0.0655 - 1.0086i	-0.0489 + 0.9929i	0.8427 - 0.0000i
Ln Min=0.77mH	-1.0267 - 0.0007i	0.8751 - 0.3942i	0.8800 + 0.3792i

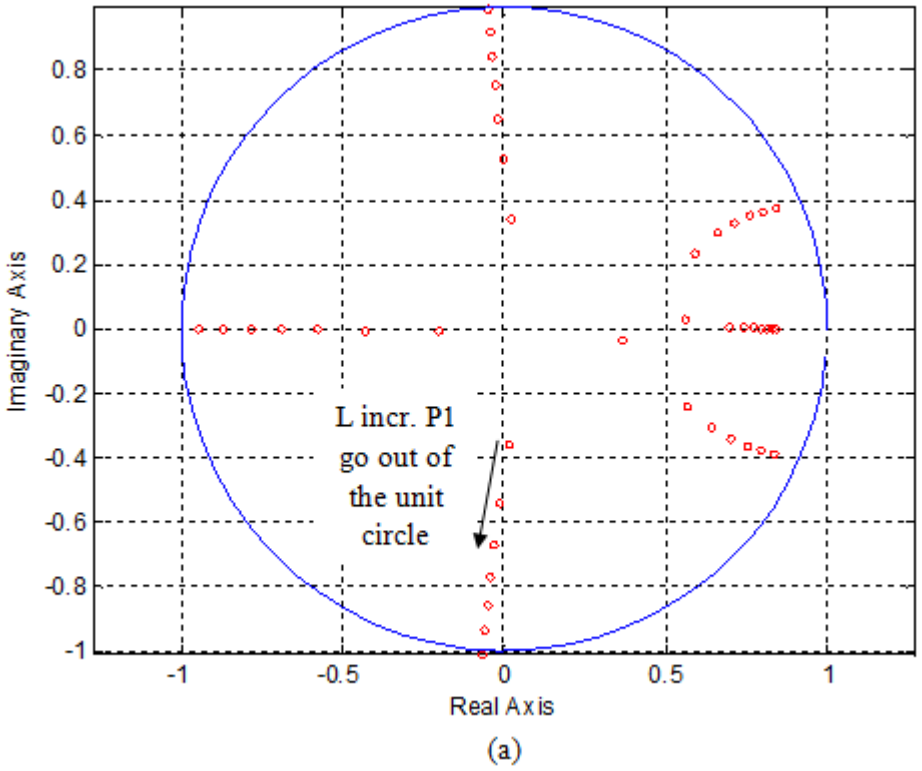

(a)

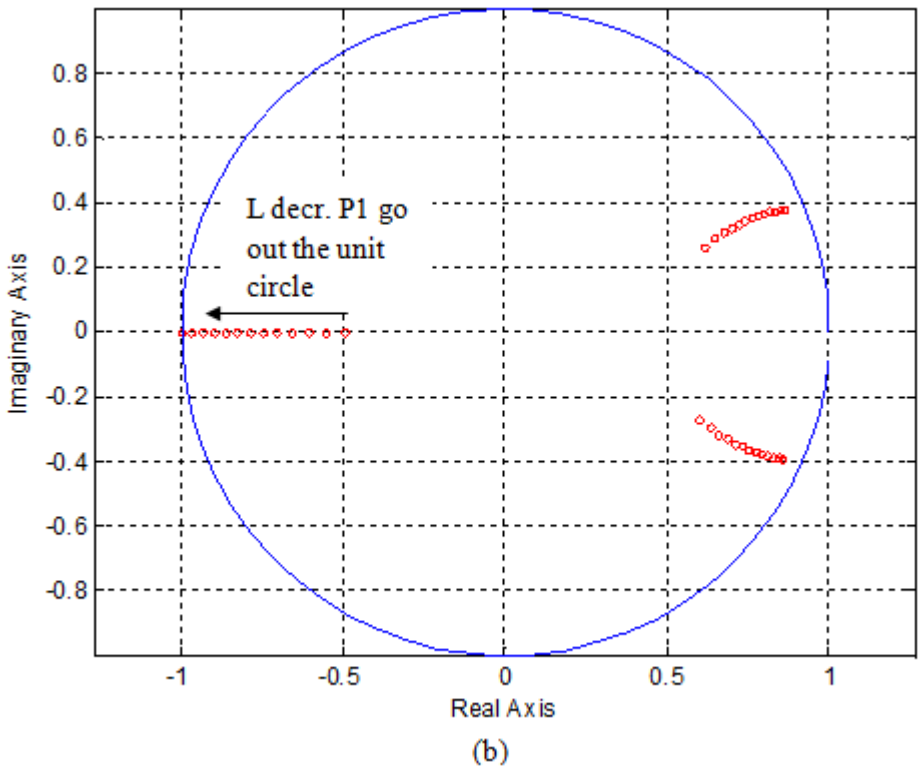

(b)

Figure 5.5: Pole Locations of the Disturbance Estimator for Unstable States. (a) L_n Greater Than L_{Max} and (b) L_n Less Than L_{Min} and

5.4.2 Change in Estimator Gains and Unchanged Inductor

In this case we shall make the actual inductor value constant at the nominal inductor actual value $L = 3mH$ and change the disturbance estimator gains l_1, l_2 . This gives also two states, the first being stable, where we change the gains until their max values which make the system stable. Second case is unstable. In this state we have two cases, firstly, we change the value of l_1 until the system becomes unstable, while l_2 is kept constant. Lastly, we change the value of l_2 until the system becomes unstable, while l_1 is kept constant.

Stable State

In this case all the poles are inside the unit circle. Table 5.3 contains the values that keep the system stable. Figure 5.6 shows the pole locations for the stable state, where all the poles are inside the unit circle with the max possible change of the estimator gains.

Table 5.4: Pole Values and Estimator Gains with Actual Filter Inductor Value

L	l_1	l_2	λ_1	λ_2	λ_3
3mH	2.08	-10	-0.9983 - 0.0164i	0.0000 - 0.0000i	0.9166 + 0.0007i

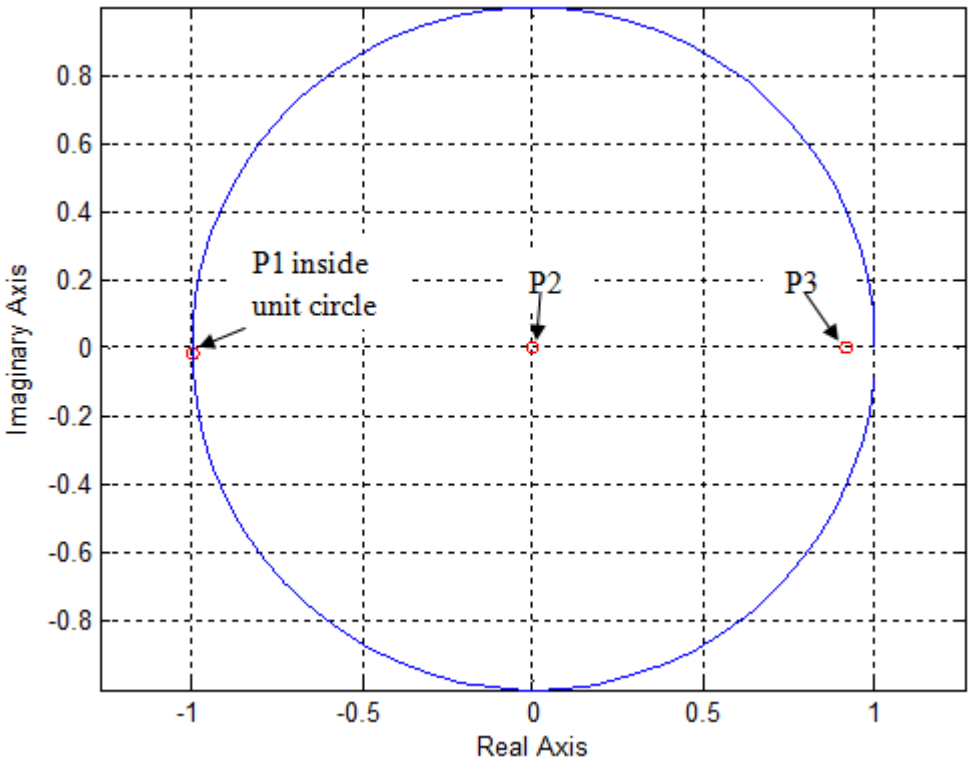

Figure 5.6: Pole Locations on Unit Circle at Stable State Where Estimator Gains are Changed and Filter Inductance is Unchanged

Unstable State

In this case we have two possible changes that make the system unstable. First we assume l_2 is constant and change l_1 until the system becomes unstable. Table 5.4, gives the pole values and estimator gains with the actual filter inductance value. Figure 5.7.a, shows the pole locations, where we observe that one of the poles is out of the unit circle which is enough to make the system unstable. Second state corresponds to adjusting the value of l_2 while l_1 is to be kept constant. Table 5.5 has the values of the gains that make the estimator unstable. So Table 5.4 and 5.5 and Figure 5.7(a, b) clearly describe the effects of the gains on the system trajectory, where one stable and the other one is unstable.

Table 5.5: Pole Values and Estimator Gains Change l_1

L	l_1	l_2	λ_1	λ_2	λ_3
3mH	2.17	-20	-1.0055 - 0.0171i	-0.0000 + 0.0000i	0.8338 + 0.0014i

Table 5.6: Pole Values and Estimator Gains Change l_2

L	l_1	l_2	λ_1	λ_2	λ_3
3mH	1.27	-76	0.3588 -0.9365i	0.3695 +0.9208i	0.0000 - 0.0000i

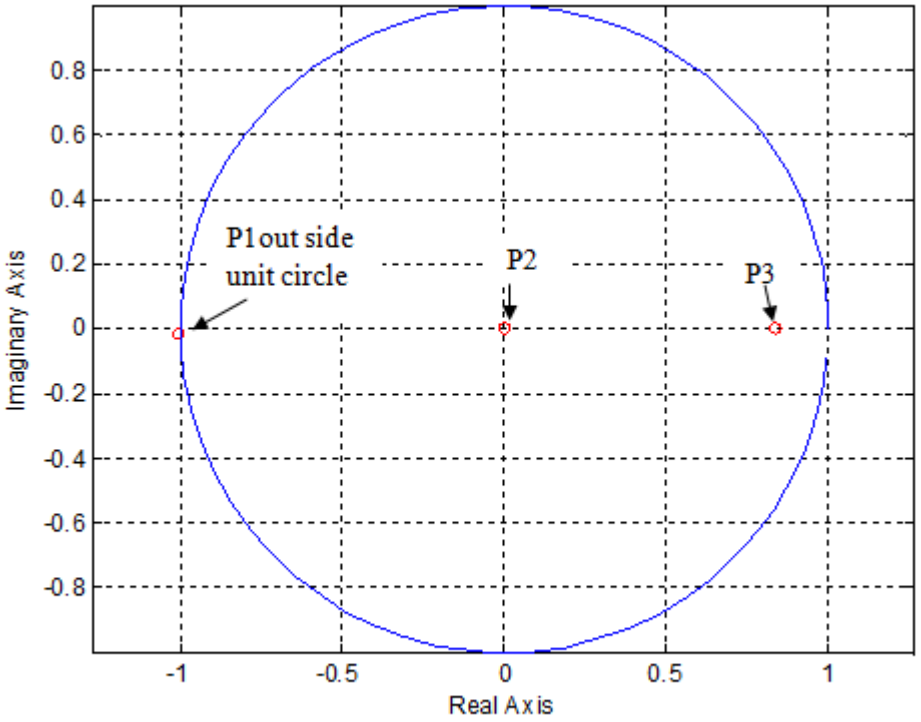

(a)

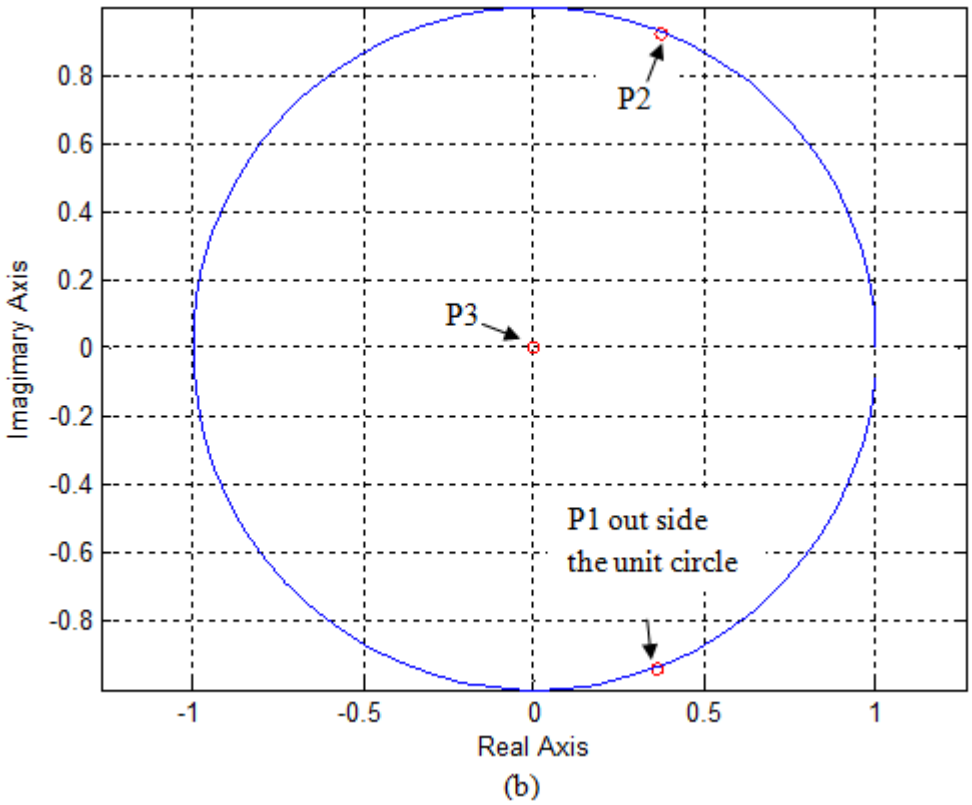

(b)

Figure 5.7: Pole Locations with Change in Gains for Unstable State (a) change in l_1 and (b) Change in l_2

Chapter 6

CONCLUSIONS AND FUTURE WORK

6.1 Conclusions

In this thesis, the disturbance estimator based predictive current control of grid-connected inverter is adopted. Firstly, we conclude that the disturbance control reduces the effects of uncertainties in the parameter values of the $R-L$ filter via a feedback from the inverter output voltage to reduce the error between the actual and desired current. Secondly, the disturbance control strategy allows the inverter to be easily synchronized with the grid. This is achieved by extracting the grid angle using PLL, via the reactive estimation component of the disturbance. The thesis also discusses stability analysis of the control strategy. The system is found to be stable while changing the value of the inductor from -65% to +65% of the actual value, keeping the estimator gains unchanged. Also the values of the estimator gains have been changed while keeping the inductor value unchanged and still having a stable system again.

The disturbance control system uses no sensors for the prediction of any type. This reduces the cost and the equipment of the overall system. The control system is found to be robust against the disturbance effects which led to high performance and high efficiency.

6.2 Future Work

In the future work, we wish to develop the predictive current control strategy to involve the maximum possible change on the inductance value of the filter, by increase the estimator sensitivity that gives ability to detect any disturbance. Also we propose to connect other types of filter such as L-C or L-C-L, that may help to eliminate the effective low order harmonics and gives low THD.

REFERENECES

[1] B. M. Wilamowski & J. D. Irwin, *The Industrial Electronics Handbook-Power Electronic and Motor Drives*, 2nd ed., CRC Press: Taylor & Francis, 2011.

[2] B. K. Bose, *Modern Power Electronics and AC Drives*, Prentice Hall, Upper Saddle River, 2002.

[3] M. H. Rashid, *Power Electronics Handbook*, Academic Press, 2001.

[4] H. R. Pouya, & H. Mokhtari, *Control of Parallel Three Phase Inverter Using Optimal Control and SVPWM Technique*, Proc. of 2009.

[5] E. Hendawi, F. Khater, & A. Shaltout, "Analysis, Simulation and Implementation of Space Vector Pulse Width Modulation Inverter," *Proceedings of the 9th WSEAS International Conf., on Applications of Electrical Engineering*. 2010.

[6] M. G. Judewicz, J. R. Fischer, M. A. Herran, S. A. Gonzalez, & D. O. Carrica, "A Robust Model Predictive Control for Grid-Connected Voltage-Source Inverters," *IEEE, Latin America Trans*., vol. 11, no.1, Feb. 2013.

[7] Y. R. Mohamed, & E. El-Saadany, "A Control Scheme for PWM voltage-source Distributed-Generation Inverters for Fast Load-Voltage Regulation and Effective

Mitigation of Unbalanced Voltage disturbances," *IEEE Trans. on Industrial Electronics*, vol. 55, no. 5, pp. 2073-2084, May 2008.

[8] J. Espi, J. Castello, R. Garci-Gil, G. Garcera, & E. Figueres, "An Adaptive Robust Predictive Current Control for Three Phase Grid-connected Inverters," *IEEE Trans. on Industrial Electronics*, vol. 58, no. 8, pp. 3537-3546, Aug. 2011.

[9] J. Castello, J. Espi, R. Garcia-Gil, & S. Gonzalez, "A Robust Predictive Current Control for Three-Phase Grid-Connected Inverters*,"*, *IEEE Trans. on Industrial Electronics*, vol. 56, no. 6, pp. 1993-2004, Jun. 2009.

[10] F. Blaabjerg, R. Teodorescu, M. Liserre, & A. Timbus, "Overview of Control and Grid Synchronization for Distributed Power Generation System," *IEEE Trans. on Industrial Electronics*, vol. 53, no. 5, pp. 1398-1409, Oct. 2006.

[11] P. Cortes. M. Kazmierkowski, R. Kennel, D. Quevedo, & J. Rodriguez, "Predictive Control in Power Electronics and Drives," *IEEE Trans. on Industrial Electronics*, vol. 55, no. 12, pp. 4312-4324, Dec. 2008.

[12] D. Vilathgamuwa, P.Loh, & Y. Li, "Protection of Microgrids During Utility Voltage sags," *IEEE Trans. on Industrial Electronics*, vol. 53, no. 5, pp. 1427-1436, Oct. 2006.

[13] G. Bode, P. C. Loh, M. Newman, & D. Holmes, "An Improved Robust Predictive Current Regulation Algorithm," *IEEE Trans. on Industrial Applications*, vol. 41, no. 6, pp. 1720–1733, Nov./Dec. 2005.

[14] D. Holmes, & D. Martin, "Implementation of a Direct Digital predictive Current Controller for Single and Three Phase Voltage Source Inverters," *IEEE IAS Conference Annual Meeting*, vol. 2, pp. 906–913, Oct. 1996.

[15] Y. Fang & Y. Xing, "Design and Analysis of Three-Phase Reversible High Power-Factor Correction Based on Predictive current Controller," *IEEE Trans. Industrial Electronics*, vol. 55, no. 12, pp. 4391–4397, Dec. 2008.

[16] A. H. Mario, R. F. Jonatan, A. G. Sergio, G. J. Marcos, & O. C. Daniel, "Adaptive Dead-Time Compensation for Grid-Connected PWM Inverter of Single-Stage PV System," *IEEE Trans. on Power Electronics*, vol. 28, no.6, pp. 2816-2825, June 2013.

[17] J. W. Choi, & S.K. Sul, "A New Compensation Strategy Reducing Voltage/Current Distortion in PWM VSI System Operation With Low Output Voltages," *IEEE Trans. on Industrial Application*, vol. 31, no 5, pp. 1001-1008, Sep./oct.1995.

[18] I. Atif, M. A. Sk, A. K. Mohammad, & A.-R. Haitham, "Generalised Simulation and Experimental Implementation of Space Vector PWM Technique of a Three-Phase Voltage Source Inverter," *International Journal of Engineering, Science Technology*, vol. 2, no. 1, pp. 1-12, 2010.

[19] R. Rajendran, & N. Devarajan, "FPGA Implementation of Space Vector PWM Technique for Voltage Source Inverter Fed Induction Motor Drive," *IEEE Second International Conference, in Computer &Electrical Engineering*, vol. 2, pp. 422-426, Dec. 2009.

[20] K-J Lee, B-G Park, R-Y Kim, & D-S Hyun, "Robust Predictive Current Controller based on a Disturbance Estimator in a Three-Phase Grid-Connected Inverter*," IEEE Trans. Power Electronics*, vol. 27, no. 1, pp. 276-283, Jun. 2012.

[21] H.-T. Moon, H.-S. Kim, & M.-J. Youn, "A Discrete-Time Predictive Current Control for PMSM," *IEEE Trans. Power Electronics*, vol. 18, no. 1, pp. 464-472, Jun. 2003.

[22] S. Kouro, P. Cortes, R. Vargas, U. Ammann, & J. Rodriguez, "Model Predictive Control-a Simple and Powerful Method to Control Power Converters," *IEEE Trans. Industrial Electronics*, vol. 56, no. 6,pp. 1826-1838, Jun. 2009.

[23] O. Kukrer, "Discrete-Time Current Control Voltage-Fed Three Phase PWM Inverter*," IEEE Trans. Power Electronics*, vol. 11, no. 2, pp. 260-269, Mar. 1996.

[24] G. F. Franklin, J. D. Powell, & A. Emami-Naeini, "Feedback Control of Dynamic System" *4th ed. Reading, MA: Addison-Wesley*,2002.

[25] H. Fainan, & C. Roger, ”A Robust PLL for Grid Interactive Voltage Source Converters,” *14th International Power Electronics and Motion Control Conference*, EPE-PEMC 2010.

[26] V. Kaura, & V. Blasko, ”Operation of Phase Looked Loop System Under Distorted Utility Condition*,” IEEE Trans. on Industry Applications*, vol. 33, no. 1 Jun./Feb. 1997.

APPENDICES

Appendix A: Derivation of Equation (4.33)

The actual current at one sample is;

$$i_{dq}(t_{k+1}) = \left(1 - \frac{T_s}{L}(R + jwL)\right) i_{dq}(t_k) - \frac{T_s}{L} f_{dq}(t_k) + \frac{T_s}{L} V_{odq}(t_k) \tag{1A}$$

$$V_{odq}(t_k) = \left(R_n + jwL - \frac{L_n}{T_s}\right) \hat{i}_{dq}(t_k) + \frac{L_n}{T_s} i^*_{dq}(t_{k+1}) + \hat{f}_{dq}(t_k) \tag{2A}$$

Substitute (2A) in (1A);

$$\begin{aligned} i_{dq}(t_{k+1}) = & \left(1 - \frac{T_s}{L}(R + jwL)\right) i_{dq}(t_k) - \frac{T_s}{L} f_{dq}(t_k) \\ & + \left(\frac{T_s}{L}\left(R_n + jwL - \frac{L_n}{T_s}\right) \hat{i}_{dq}(t_k)\right) + + \frac{L_n}{T_s} i^*_{dq}(t_{k+1}) + \hat{f}_{dq}(t_k)) \end{aligned} \tag{3A}$$

The state space equation for the estimator is;

$$\begin{aligned} \begin{bmatrix} \hat{i}_{dq}(t_{k+1}) \\ \hat{f}_{dq}(t_{k+1}) \end{bmatrix} = & \begin{bmatrix} 1 - T_s(R_n + jwL_n)/L_n & -T_s/L_n \\ 0 & 1 \end{bmatrix} \begin{bmatrix} \hat{i}_{dq}(t_k) \\ \hat{f}_{dq}(t_k) \end{bmatrix} \\ & + \begin{bmatrix} T_s/L_n \\ 0 \end{bmatrix} \left(R_n + jwL - \frac{L_n}{T_s}\right) \hat{i}_{dq}(t_k) + \frac{L_n}{T_s} i^*_{dq}(t_{k+1}) + \hat{f}_{dq}(t_k) \\ & + \begin{bmatrix} l_1 \\ l_2 \end{bmatrix} \times \left(i_{dq}(t_k) - [1 \;\; 0] \begin{bmatrix} \hat{i}_{dq}(t_k) \\ \hat{f}_{dq}(t_k) \end{bmatrix} \right) \end{aligned} \tag{4A}$$

After simplification equation (4A) we get;

$$\hat{i}_{dq}(t_{k+1}) = l_1 i_{dq}(t_k) - l_1 \hat{i}_{dq}(t_k) + l_1 i^*_{dq}(t_{k+1}) \tag{5A}$$

$$\hat{f}_{dq}(t_{k+1}) = f_{dq}(t_k) + l_2 (i_{dq}(t_k) - \hat{i}_{dq}(t_k)) \tag{6A}$$

The equation that description the combine system is;

$$\begin{bmatrix} i_{dq}(t_{k+1}) \\ \hat{i}_{dq}(t_{k+1}) \\ \hat{f}_{dq}(t_{k+1}) \end{bmatrix} = \begin{bmatrix} 1-\frac{T_s}{L}(R+jwL) & \frac{T_s}{L}\left(R_n+jwL_n\right)-\frac{L_n}{L} & \frac{T_s}{L} \\ l_1 & -l_1 & 0 \\ l_2 & -l_2 & 1 \end{bmatrix} \begin{bmatrix} i_{dq}(t_k) \\ \hat{i}_{dq}(t_k) \\ \hat{f}_{dq}(t_k) \end{bmatrix} \quad (7A)$$

$$+ \begin{bmatrix} L_n / L & -(T_s / L) \\ 1 & 0 \\ 0 & 0 \end{bmatrix} \begin{bmatrix} i^*_{dq}(t_{k+1}) \\ f_{dq}(t_k) \end{bmatrix}$$

Appendix B: Matlab Code of Plotting Poles Locations.

```
for C=1:0.6:8.8

Ln=(0.00022*C)+0.00055;

l1=1.27;

l2=-20;

z=1-(Ts/L)*(R+i*W*L);

y=((Ts/L)*(Rn+i*W*Ln))-Ln/L;

Q=Ts/L;

J=[z y Q ;G1 -G1 0 ;G2 -G2 1];

BB=eig(J)

ei=real(eig(J));

zi=imag(eig(J));

X=subs(ei)';

Y=subs(zi)';

H=scatter(X,Y,10,'r');

grid on

th=0:0.1:2*pi;

x=cos(th);

y=sin(th);

plot(x,y)

axis equal

hold on

    end
```